Eur. Phys. J. E **31**, 3–24 (2010)
DOI 10.1140/epje/i2010-10543-1

THE EUROPEAN PHYSICAL JOURNAL E

Regular Article

Heat transfer between elastic solids with randomly rough surfaces

B.N.J. Persson[1,a], B. Lorenz[1], and A.I. Volokitin[1,2]

[1] IFF, FZ-Jülich, 52425 Jülich, Germany
[2] Samara State Technical University, 443100 Samara, Russia

Received 13 August 2009 and Received in final form 30 October 2009
Published online: 20 January 2010 –

Abstract. We study the heat transfer between elastic solids with randomly rough surfaces. We include both the heat transfer from the area of real contact, and the heat transfer between the surfaces in the non-contact regions. We apply a recently developed contact mechanics theory, which accounts for the hierarchical nature of the contact between solids with roughness on many different length scales. For elastic contact, at the highest (atomic) resolution the area of real contact typically consists of atomic (nanometer) sized regions, and we discuss the implications of this for the heat transfer. For solids with very smooth surfaces, as is typical in many modern engineering applications, the interfacial separation in the non-contact regions will be very small, and for this case we show the importance of the radiative heat transfer associated with the evanescent electromagnetic waves which exist outside of all bodies.

1 Introduction

The heat transfer between solids is a topic of great importance. Classical applications include topics such as cooling of microelectronic devices, spacecraft structures, satellite bolted joints, nuclear engineering, ball bearings, tires and heat exchangers. Other potential applications involve microelectromechanical systems (MEMS). Heat transfer is also of crucial importance in friction and wear processes, *e.g.*, rubber friction on hard and rough substrates depends crucially on the temperature increase in the rubber-countersurface asperity contact regions [1].

A large number of papers have been published on the heat transfer between randomly rough surfaces [2]. However, most of these studies are based on asperity contact models such as the model of Greenwood and Williamson (GW) [3]. Recent studies have shown that the GW-model (and other asperity contact models [4]) are very inaccurate [5–7], mainly because of the neglect of the long-range elastic coupling [8]. That is, if an asperity is pushed downwards somewhere, the elastic deformation field extends a long distance away from the asperity, which will influence the contact involving other asperities further away [9]. This effect is neglected in the GW theory, but it is included in the contact mechanics model of Persson [10–15], which we use in the present study. In addition, in the GW model the asperity contact regions are assumed to be circular (or elliptical) while the actual contact regions (at high enough resolution) have fractal-like boundary lines [15–17], see fig. 1. Thus, because of their complex nature, one should try to avoid involving directly the nature of the contact regions when studying contact mechanics problems, such as the heat or electric contact resistance. The approach we use in this paper does not directly involve the nature of the contact regions. Finally, we note that for elastically hard solids the area of real (atomic) contact A may be a very small fraction of the nominal or apparent contact area A_0, even at high nominal squeezing pressures [18,19].

Another important discovery in recent contact mechanics studies is that for elastic contact, the contact regions observed at atomic resolution may be just a few atoms wide, *i.e.*, the diameter of the contact regions may be of the order of $\sim 1\,\mathrm{nm}$ [20–22]. The heat transfer via such small junctions may be very different from the heat transfer through macroscopic-sized contact regions, where the heat transfer usually is assumed to be proportional to the linear size of the contact regions (this is also the prediction of the macroscopic heat diffusion equation), rather than the contact area. In particular, if the typical phonon wavelength involved in the heat transfer becomes larger than the linear size of the contact regions (which will always happen at low enough temperature) the effective heat transfer may be strongly reduced. Similarly, if the phonons mean free path is longer than the linear size of the contact regions, ballistic (phonon) energy transfer may occur which cannot be described by the macroscopic heat diffusion equation. These effects are likely to be of crucial importance in many modern applications involving micro- (or nano-) sized objects, such as MEMS, where just a few atomic-sized contact regions may occur. However, for

[a] e-mail: b.persson@fz-juelich.de

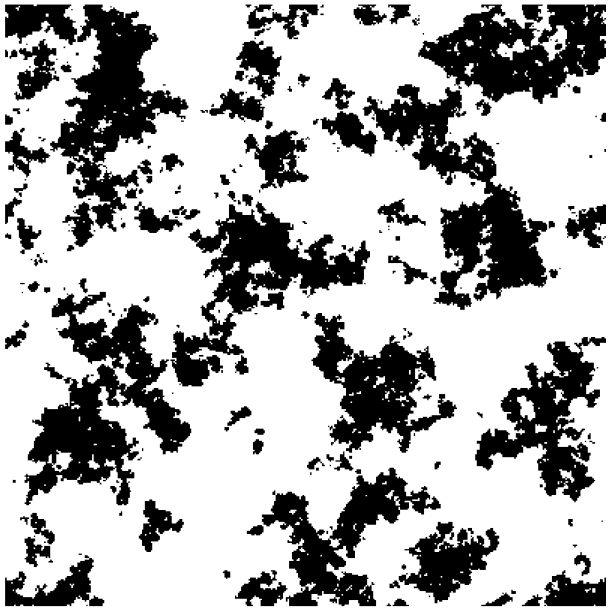

Fig. 1. The black area is the contact between two elastic solids with randomly rough surfaces. For surfaces which have fractal-like roughness the whole way down to the atomic length scale, the contact at the highest magnification (atomic resolution) typically consists of nanometer-sized atomic clusters. The result is obtained using Molecular Dynamics (MD), but since there is no natural length scale in elastic continuum mechanics the picture could also be the contact observed between two macroscopic elastic solids. Adapted from ref. [15].

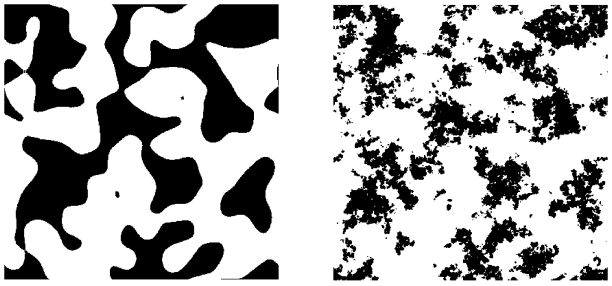

Fig. 2. The contact region (black area) between two elastic solids observed at low (left) and high (right) magnification. The contact resistance depends mainly on the long-wavelength roughness, and can usually be calculated accurately from the nature of the contact observed at low magnification (left).

macroscopic solids the thermal (and electrical) contact resistance is usually very insensitive to the nature of the contact regions observed at the highest magnification, corresponding to atomistic (or nanoscale) length scales. In fact, the heat transfer is determined mainly by the nature of the contact regions observed at lower magnification where the contact regions appear larger (see sect. 5 and [23,24]), see fig. 2. For example, in sect. 2.2.1 we show that for self-affine fractal surfaces the contact resistance depends on the range of surface roughness included in the analysis as $\sim r(H) - (q_0/q_1)^H$, where q_0 and q_1 are the smallest and the largest wave vector of the surface roughness included in the analysis, respectively, and H is the Hurst exponent related to the fractal dimension via $D_{\rm f} = 3-H$. The number $r(H)$ depends on H but is of the order of unity. In a typical case $H \approx 0.8$, and including surface roughness over one wave vector decade $q_0 < q < q_1 = 10q_0$ results in a heat resistance which typically is only $\sim 10\%$ smaller than obtained when including infinitely many decades of length scales (*i.e.*, with $q_1 = \infty \times q_0$). At the same time the area of real contact approaches zero as $q_0/q_1 \to 0$. Thus, there is in general no relation between the area of real contact (which is observed at the highest magnification, and which determines, *e.g.*, the friction force in most cases), and the heat (or electrical) contact resistance between the solids. One aspect of this in the context of electric conduction was pointed out a long time ago [25]: if an insulating film covers the solids in the area of real contact, and if electrical contact occurs by a large number of small breaks in the film, the resistance may be almost as low as with no film. Similarly, the thermal contact resistance of macroscopic solids usually does not depend on whether the heat transfer occurs by diffusive or ballistic phonon propagation, but rather the contact resistance is usually determined mainly by the nature of the contact regions observed at relative low magnification.

Note that as H decreases towards zero (or the fractal dimension $D_{\rm f} \to 3$) one needs to include more and more decades in the length scales in order to obtain the correct (or converged) contact resistance, and for $H = 0$ (or $D_{\rm f} = 3$) it is necessary to include the roughness on the whole way down to the atomic length scale (assuming that the surfaces remain fractal-like with $H = 0$ the whole way down to the atomic length scale). Most natural surfaces and surfaces of engineering interest have (if self-affine fractal) $H > 0.5$ (or $D_{\rm f} < 2.5$), *e.g.*, surfaces prepared by crack propagation or sand blasting typically have $H \approx 0.8$, and in these cases the contact resistance can be calculated accurately from the (apparent) contact observed at relatively low magnification. However, some surfaces may have smaller Hurst exponents. One interesting case is surfaces (of glassy solids) with frozen capillary waves [14,26] (which are of great engineering importance [26]), which have $H = 0$. The heat transfer between such surfaces may be understood only by studying the system at the highest magnification corresponding to atomic resolution.

In this paper we will consider the heat transfer between (macroscopic-sized) solids in the light of recent advances in contact mechanics. We will study the contribution to the heat transfer not just from the area of real contact (observed at atomic resolution), but also the heat transfer across the area of non-contact, in particular the contribution from the fluctuating electromagnetic field, which surrounds all solid objects [27,28]. For high-resistivity materials and for hard and very flat surfaces, such as those involved in many modern applications, *e.g.*, MEMS applications, this non-contact radiative heat transfer may in fact dominate in the total heat transfer (at least under vacuum condition). We note that for flat surfaces (in vacuum) separated by a distance d larger than the thermal length $d_T = c\hbar/k_{\rm B}T$, the non-contact heat transfer is given by the classical Stefan-Boltzman law, and is

independent of d. However, for very short distances the contribution from the evanescent electromagnetic waves to the heat transfer will be many orders of magnitude larger than the contribution from propagating electromagnetic waves (as given by the Stefan-Boltzman law) [27].

In most applications (but not in spacecraft applications) one is interested in the heat transfer between solid objects located in the normal atmosphere and sometimes in a fluid. Most solid objects in the normal atmosphere have organic and water contamination layers, which may influence the heat transfer for at least two reasons: (a) Thin (nanometer) contamination layers may occur at the interface in the asperity contact regions, which will affect the acoustic impedance of the contact junctions, and hence the propagation of phonons between the solids (which usually is the origin of the heat transfer, at least for most non-metallic systems). (b) In addition, capillary bridges may form in the asperity contact regions and effectively increase the size of the contact regions and increase the heat transfer. In the normal atmosphere heat can also be transferred between the non-contact regions via heat diffusion or (at short separation) ballistic processes in the surrounding gas. For larger separations convective processes may also be important.

In the discussion above we have assumed that the solids deform elastically and we have neglected the adhesional interaction between the solids. The contact mechanics theory of Persson can also be applied to cases where adhesion and plastic flow are important, and we will briefly study how this may affect the heat transfer. Most solids have modified surface properties, *e.g.*, metals are usually covered by thin oxide layers with very different conductivities than the underlying bulk materials. However, as mentioned above, this may not have any major influence on the contact resistance.

Recently, intense research has focused on heat transfer through atomic or molecular-sized junctions [29–31]. In light of the discussion presented above, this topic may also be important for the heat transfer between solids, because of the nanometer-sized nature of the contact regions between solids with random roughness.

This paper is organized as follows: In sect. 2 we describe the theory for heat transfer between two solids with randomly rough surfaces. We consider both the heat flow in the area of real contact, and between the surfaces in the non-contact area. Section 3 presents a short review of the contact mechanics theory which is used to obtain the quantities (related to the surface roughness) which determine the heat transfer coefficient. In sect. 4 we present numerical results. In sect. 5 we discuss the influence of plastic flow and adhesion on the heat transfer. Section 6 presents an application to the heat transfer between tires and the air and road surface. In sect. 7 we discuss a new experiment. In sect. 8 we present experimental results. In sect. 9 we point out that the developed theory can also be applied to the electric contact resistance. Section 10 contains the summary and conclusion. Appendix A-E present details related to the theory development and some other general information relevant to the present study.

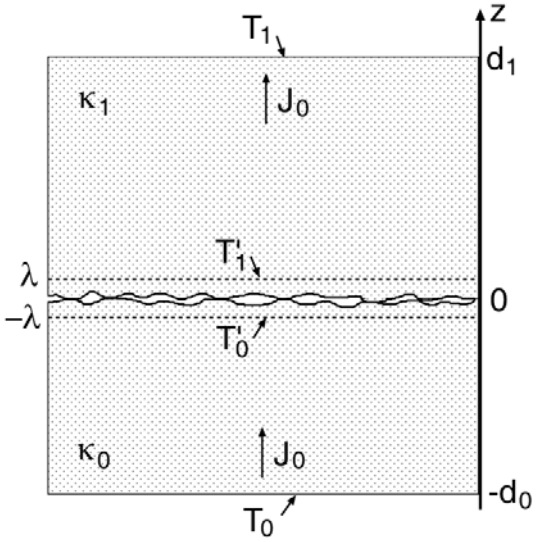

Fig. 3. Two elastic solids with nominally flat surfaces squeezed together with the nominal pressure p_0. The heat current $J_z(\mathbf{x})$ at the contacting interface varies strongly with the coordinate $\mathbf{x} = (x, y)$ in the xy-plane. The average heat current is denoted by $J_0 = \langle J_z(\mathbf{x}) \rangle$.

2 Theory

2.1 Heat transfer coefficient

Consider two elastic solids (rectangular blocks) with randomly rough surfaces squeezed in contact as illustrated in fig. 3. Assume that the temperature at the outer surfaces $z = -d_0$ and $z = d_1$ is kept fixed at T_0 and T_1, respectively, with $T_0 > T_1$. Close to the interface the heat current will vary rapidly in space, $\mathbf{J} = \mathbf{J}(\mathbf{x}, z)$, where $\mathbf{x} = (x, y)$ denote the lateral coordinate in the xy-plane. Far from the interface we will assume that the heat current is constant and in the z-direction, *i.e.*, $\mathbf{J} = J_0 \hat{z}$. We denote the average distance between the macro asperity contact regions by λ (see ref. [14]). We assume that $\lambda \ll L$, where L is the linear size of the apparent contact between the elastic blocks. The temperature a distance $\sim \lambda$ from the contacting interface will be approximately independent of the lateral coordinate $\mathbf{x} = (x, y)$ and we denote this temperature by T_0' and T_1' for $z = -\lambda$ and $z = \lambda$, respectively. The heat current for $|z| \gg \lambda$ is independent of $\mathbf{x}$ and can be written as (to zero order in λ/d_0 and λ/d_1)

$$J_0 = -\kappa_0 \frac{T_0' - T_0}{d_0} = -\kappa_1 \frac{T_1 - T_1'}{d_1}\,, \tag{1}$$

where κ_0 and κ_1 are the heat conductivities of the two solid blocks. We assume that the heat transfer across the interface is proportional to $T_0' - T_1'$ and we define the heat transfer coefficient α so that

$$J_0 = \alpha(T_0' - T_1'). \tag{2}$$

Combining (1) and (2) gives

$$J_0 = \frac{T_0 - T_1}{d_0\kappa_0^{-1} + d_1\kappa_1^{-1} + \alpha^{-1}}\,. \tag{3}$$

This equation is valid as long as $\lambda \ll L$ and $\lambda \ll d_0$, d_1. Note that α depends on the macroscopic (or nominal) pressure which acts at the interface. Thus if the macroscopic pressure is non-uniform, as is the case in many practical applications, *e.g.*, when a ball is squeezed against a flat surface, one need to include the dependence of α on $\mathbf{x}$. Thus in general

$$J(\mathbf{x}) = \alpha(\mathbf{x})[T_0'(\mathbf{x}) - T_1'(\mathbf{x})]. \tag{4}$$

One expects the contribution to α from the area of real contact to be proportional to the heat conductivity κ (for simplicity we assume here two solids of the same material). Assuming only elastic deformation, contact mechanics theories show that for low enough squeezing pressure p_0, the area of real contact is proportional to p_0, and the size distribution of contact regions (and the interfacial stress probability distribution) are independent of p_0. Thus one expects that α is proportional to p_0. For randomly rough surfaces the contact mechanics depends only on the (effective) elastic modulus E^* and on the surface roughness power spectrum $C(q)$. Thus the only way to construct a quantity which is proportional to $p_0\kappa$ and with the same dimension as $J_0/\Delta T$, using the quantities which characterize the problem, is

$$\alpha \approx \frac{p_0\kappa}{E^* u_0}\,,$$

where u_0 is a length parameter which is determined from the surface roughness power spectrum $C(q)$. For self-affine fractal surfaces, $C(q)$ depends only on the root-mean-square roughness $h_{\rm rms}$, the fractal dimension $D_{\rm f}$ which is dimensionless, and on the low and high cut-off wave vectors q_0 and q_1. Thus in this case $u_0 = h_{\rm rms} f(D_{\rm f}, q_0/q_1, q_0 h_{\rm rms})$. This result is consistent with the analysis presented in sect. 2.2.1. Using the GW theory results in an expression for α of the form given above, but with a different function f which now (even for low squeezing pressures) also depends on p_0/E^* (see, *e.g.*, ref. [32]).

2.2 Calculation of α

The heat current $\mathbf{J}$ and the heat energy density Q are assumed to be given by

$$\mathbf{J} = -\kappa\nabla T, \qquad Q = \rho C_V T,$$

where κ is the heat conductivity, ρ the mass density and C_V the heat capacitivity. We consider a steady-state condition where Q is time independent. Thus the heat energy continuity equation,

$$\nabla\cdot\mathbf{J} + \frac{\partial Q}{\partial t} = 0,$$

reduces to

$$\nabla^2 T = 0.$$

We assume that the surface roughness at the interface is so small that when solving the heat flow equation we can consider the surfaces as flat. However the heat flow across the interface will be highly non-uniform and given by the heat current $J_z(\mathbf{x})$ (we assume $|\nabla h| \ll 1$, where $h(\mathbf{x})$ is the surface height profile). Let us first study the heat flow in the upper solid. We can take into account the heat flow from the lower solid by introducing a heat source at the interface $z = 0$, *i.e.*

$$\nabla^2 T = -2J_z(\mathbf{x})\delta(z)/\kappa_1. \tag{5}$$

Similarly, when studying the temperature in the lower solid we introduce a heat sink on the surface $z = 0$, so that

$$\nabla^2 T = 2J_z(\mathbf{x})\delta(z)/\kappa_0. \tag{6}$$

Let us first study the temperature for $z > 0$. We write

$$J_z(\mathbf{x}) = \int {\rm d}^2q\, J_z(\mathbf{q}) e^{i\mathbf{q}\cdot\mathbf{x}}, \tag{7}$$

$$J_z(\mathbf{q}) = \frac{1}{(2\pi)^2}\int {\rm d}^2x\, J_z(\mathbf{x}) e^{-i\mathbf{q}\cdot\mathbf{x}}, \tag{8}$$

where $\mathbf{q} = (q_x, q_y)$ is a 2D wave vector. From (5) we get

$$T(\mathbf{x}, z) = T_1 - \frac{1}{\kappa_1} J_0(z - d_1) - \frac{1}{\pi\kappa_1}\int {\rm d}^2q{\rm d}k \frac{\Delta J_z(\mathbf{q})}{-q^2 - k^2} e^{i(\mathbf{q}\cdot\mathbf{x} + kz)}, \tag{9}$$

where k is the z-component of the wave vector. In (9), $J_0 = \langle J_z(\mathbf{x})\rangle$ is the average heat current and

$$\Delta J_z(\mathbf{x}) = J_z(\mathbf{x}) - J_0. \tag{10}$$

Performing the k-integral in (9) gives

$$T(\mathbf{x}, z) = T_1 - \frac{1}{\kappa_1} J_0(z - d_1) + \frac{1}{\kappa_1}\int {\rm d}^2q\, \frac{1}{q}\Delta J_z(\mathbf{q}) e^{i\mathbf{q}\cdot\mathbf{x} - qz}. \tag{11}$$

Similarly, one obtains for the temperature field for $z < 0$

$$T(\mathbf{x}, z) = T_0 - \frac{1}{\kappa_0} J_0(z + d_0) - \frac{1}{\kappa_0}\int {\rm d}^2q\, \frac{1}{q}\Delta J_z(\mathbf{q}) e^{i\mathbf{q}\cdot\mathbf{x} + qz}. \tag{12}$$

Let us define

$$\psi(\mathbf{x}) = T(\mathbf{x}, -0) - T(\mathbf{x}, +0).$$

Using (11) and (12), we get

$$\psi(\mathbf{x}) = T_0 - T_1 - \left(\frac{d_0}{\kappa_0} + \frac{d_1}{\kappa_1}\right) J_0 - \frac{1}{\kappa}\int {\rm d}^2q\, \frac{1}{q}\Delta J_z(\mathbf{q}) e^{i\mathbf{q}\cdot\mathbf{x}}, \tag{13}$$

where

$$\frac{1}{\kappa} = \frac{1}{\kappa_0} + \frac{1}{\kappa_1}\,. \tag{14}$$

From (13) we get

$$\psi(\mathbf{q}) = M\delta(\mathbf{q}) - \frac{1}{\kappa q}\Delta J_z(\mathbf{q}), \tag{15}$$

where

$$M = T_0 - T_1 - \left(\frac{d_0}{\kappa_0} + \frac{d_1}{\kappa_1}\right) J_0. \tag{16}$$

We will now consider two different cases:

2.2.1 Heat flow through the area of real contact

Let us consider the area of real contact. In the contact region $J_z(\mathbf{x})$ will be non-zero but $\psi(\mathbf{x}) = T(\mathbf{x}, +0) - T(\mathbf{x}, -0)$ will vanish. On the other surface area $J_z(\mathbf{x})$ will vanish. Thus we must have

$$J_z(\mathbf{x})\psi(\mathbf{x}) = 0$$

everywhere. This implies

$$\int \mathrm{d}^2q'\, J_z(\mathbf{q}-\mathbf{q}')\psi(\mathbf{q}') = 0 \tag{17}$$

for all $\mathbf{q}$. Combining (15) and (17) gives

$$MJ_z(\mathbf{q}) - \frac{1}{\kappa}\int \mathrm{d}^2q' \frac{1}{q'} J_z(\mathbf{q}-\mathbf{q}')\Delta J_z(\mathbf{q}') = 0.$$

The ensemble average of this equation gives

$$M\langle J_z(\mathbf{q})\rangle - \frac{1}{\kappa}\int \mathrm{d}^2q' \frac{1}{q'}\langle J_z(\mathbf{q}-\mathbf{q}')\Delta J_z(\mathbf{q}')\rangle = 0. \tag{18}$$

From (8) we get

$$\langle J_z(\mathbf{q}=0)\rangle = (2\pi)^{-2}A_0J_0.$$

Thus the $\mathbf{q} = \mathbf{0}$ component of (18) gives

$$MA_0J_0 - \frac{(2\pi)^2}{\kappa}\int \mathrm{d}^2q \frac{1}{q}\langle|\Delta J_z(\mathbf{q})|^2\rangle = 0, \tag{19}$$

where A_0 is the nominal contact area. Combining (16) and (19) and solving for J_0 gives an equation of the form (3) with

$$\frac{1}{\alpha} = \frac{(2\pi)^2}{\kappa}\frac{1}{A_0J_0^2}\int \mathrm{d}^2q \frac{1}{q}\langle|\Delta J_z(\mathbf{q})|^2\rangle. \tag{20}$$

We now assume that the heat current at the interface is proportional to the normal stress

$$J_z(\mathbf{x}) \approx \mu\sigma_z(\mathbf{x}). \tag{21}$$

We can also write (21) as

$$J_z(\mathbf{x})/J_0 \approx \sigma_z(\mathbf{x})/p_0, \tag{22}$$

where p_0 is the average pressure. We note that (22) implies that the current density $J_z(\mathbf{x})$ will be non-vanishing exactly where the normal stress $\sigma_z(\mathbf{x})$ is non-vanishing, which must be obeyed in the present case, where all the heat current flows through the area of real contact. We note that the heat transfer coefficient depends mainly on the spatial *distribution* of the contact area and this is exactly the same for the pressure distribution $\sigma(\mathbf{x})$ as for the current distribution $J_z(\mathbf{x})$. Thus the fact that in a particular asperity contact region the pressure $\sigma(\mathbf{x})$ is not proportional to $J_z(\mathbf{x})$ is not very important in the present context (see Appendix A and below).

Substituting (22) in (20) gives

$$\frac{1}{\alpha} \approx \frac{(2\pi)^2}{\kappa}\frac{1}{A_0p_0^2}\int \mathrm{d}^2q \frac{1}{q}\langle|\Delta\sigma_z(\mathbf{q})|^2\rangle. \tag{23}$$

We can write

$$\alpha \approx \frac{p_0^2\kappa}{E^*U_{\rm el}}\,, \tag{24}$$

where

$$U_{\rm el} = \frac{(2\pi)^2}{A_0E^*}\int \mathrm{d}^2q \frac{1}{q}\langle|\Delta\sigma(\mathbf{q})|^2\rangle \tag{25}$$

is the stored elastic energy per unit (nominal) surface area [15]. In (25) E^* is the effective elastic modulus

$$\frac{1}{E^*} = \frac{1-\nu_0^2}{E_0} + \frac{1-\nu_1^2}{E_1}\,,$$

where E_0 and ν_0 are the Young's elastic modulus and the Poisson ratio, respectively, for solid **0** and similar for solid **1**. We have shown elsewhere that for small enough load [12] $U_{\rm el} \approx u_0p_0$, where u_0 is a length of order the root-mean-square surface roughness amplitude. Thus

$$\alpha \approx \frac{p_0\kappa}{E^*u_0}\,. \tag{26a}$$

Note that for small load the squeezing pressure p_0 depends on the (average) interfacial separation $\bar{u}$ via the exponential law $p_0 \sim \exp(-\bar{u}/u_0)$. Thus the vertical stiffness $\mathrm{d}p_0/\mathrm{d}\bar{u} = -p_0/u_0$, so we can also write

$$\alpha \approx -\frac{\kappa}{E^*}\frac{\mathrm{d}p_0}{\mathrm{d}\bar{u}}\,. \tag{26b}$$

This equation is, in fact, exact (see Appendix B and ref. [24]), which shows that the heat transfer is mainly determined by the geometrical distribution of the contact area (given by the region where $\sigma_z(\mathbf{x})$ is non-vanishing), and by the thermal interaction between the heat flow through the various contact spots (see Appendix A).

The length parameter u_0 in (26a) can be calculated (approximately) from the surface roughness power spectrum $C(q)$ using [13]

$$u_0 = \sqrt{\pi}\int_{q_0}^{q_1} \mathrm{d}q\, q^2C(q)w(q),$$

where

$$w(q) = \left(\pi\int_{q_0}^{q} \mathrm{d}q' q'^3C(q')\right)^{-1/2},$$

where q_0 is the long-distance cut-off (or roll-off) wave vector and q_1 the wave vector of the shortest wavelength roughness included in the analysis. Assume that the combined surface roughness is self-affine fractal for $q_0 < q < q_1$. In this case

$$C(q) = \frac{H}{\pi}\left(\frac{h_{\rm rms}}{q_0}\right)^2 \left(\frac{q_0}{q}\right)^{2(H+1)},$$

where H is the Hurst exponent related to the fractal dimension via $D_{\rm f} = 3 - H$. Substituting this $C(q)$ into the equations above gives

$$u_0 \approx \left(\frac{2(1-H)}{\pi H}\right)^{1/2} h_{\rm rms}\left[r(H) - \left(\frac{q_0}{q_1}\right)^H\right].$$

where

$$r(H) = \frac{H}{2(1-H)}\int_1^\infty {\rm d}x\,(x-1)^{-1/2}x^{-1/[2(1-H)]}.$$

Note that $r(H)$ is of order unity (see ref. [12]). As discussed in the introduction this implies that the contact resistance in general is determined accurately by one or two decades of the longest-wavelength roughness components, and that there is no relation between the area of real contact (which is observed at the highest magnification, and which determines, *e.g.*, the friction force in most cases), and the contact resistance between the solids.

Note that from (3) it follows that one can neglect the heat contact resistance if

$$\kappa/d \ll \alpha,$$

where κ/d is the smallest of κ_0/d_0 and κ_1/d_1. Using (25) this gives

$$d \gg u_0(E^*/p_0).$$

We note that in modern high-tech applications the linear size (or thickness) d of the physical system may be very small, and in these cases the contact heat resistance may be particularly important.

If roughness occurs only on one length scale, say with wavelength λ and height h, then the pressure necessary for complete contact will be of order

$$p_0 \approx E^* h/\lambda.$$

Substituting this in (26a) gives

$$\alpha \approx \kappa/\lambda, \tag{27}$$

where we have used that $u_0 \approx h$. Thus, $\alpha^{-1} \approx \lambda\kappa^{-1}$ which is the expected result because the denominator in (3) is only accurate to zero order in $\lambda\kappa^{-1}$. (Alternatively, substituting (27) in (3) gives a term of the type $(d+\lambda)\kappa^{-1}$ which is the correct result since d in (3) should really be $d - \lambda$.)

As an example [33], consider two nominal flat steel plates (in vacuum) with thickness $d_0 = d_1 = 0.5\,{\rm cm}$ and with root-mean-square roughness $\sim 1\,\mu{\rm m}$. The plates are squeezed together with nominal pressure $p_0 = 0.1\,{\rm MPa}$. The ratio between the measured surface and bulk thermal contact resistance is about 150. Using (3) we get

$$\Delta T/J_0 = 2d_0\kappa_0^{-1} + \alpha^{-1}.$$

Thus, the (theoretical) ratio between the surface and the bulk contributions to the thermal resistance is

$$\frac{\kappa_0}{2\alpha d_0},$$

where κ_0 is the heat conductivity of the bulk steel. Using (25) with $\kappa = \kappa_0/2$ this gives

$$\frac{\kappa_0}{2\alpha d_0} = \frac{u_0}{d_0}\frac{E^*}{p_0}. \tag{28}$$

With (from theory) $u_0 \approx 1\,\mu{\rm m}$, and $E^* \approx 110\,{\rm GPa}$, $p_0 = 0.1\,{\rm MPa}$ and $2d_0 = 1\,{\rm cm}$, from (28) the ratio between the thermal surface and bulk resistance is ≈ 200, in good agreement with the experimental data.

The discussion above assumes purely elastic deformations. However, plastic flow is likely to occur in the present application at short enough length scales, observed at high magnification. Since the heat flow is determined mainly by the long-wavelength roughness components, *i.e.*, by the roughness observed at relative low magnification, when calculating the heat transfer one may often assume that the surfaces deform purely elastically, even if plastic deformation is observed at high magnification, see sect. 5.

2.2.2 Heat flow through the non-contact area

Let us now assume that

$$J_z(\mathbf{x}) = \beta(\mathbf{x})\left[T(\mathbf{x},-0) - T(\mathbf{x},+0)\right] = \beta(\mathbf{x})\psi(\mathbf{x}).$$

From (15) we get

$$\psi(\mathbf{q}) = M\delta(\mathbf{q}) - \frac{1}{\kappa q}\int {\rm d}^2q'\beta(\mathbf{q}-\mathbf{q}')\left[1 - \frac{(2\pi)^2}{A_0}\delta(\mathbf{q})\right]\psi(\mathbf{q}'). \tag{29}$$

Next, note that

$$J_0 = \frac{1}{A_0}\int {\rm d}^2x\, J_z(\mathbf{x}) = \frac{1}{A_0}\int {\rm d}^2x\,\beta(\mathbf{x})\psi(\mathbf{x}) = \frac{(2\pi)^2}{A_0}\int {\rm d}^2q\,\beta(-\mathbf{q})\psi(\mathbf{q}). \tag{30}$$

Equation (29) can be solved by iteration. The zero-order solution

$$\psi(\mathbf{q}) = M\delta(\mathbf{q}).$$

Substituting this in (30) gives

$$J_0 = M\frac{(2\pi)^2}{A_0}\beta(\mathbf{q}=\mathbf{0}) = M\bar{\beta}, \tag{31}$$

where

$$\bar{\beta} = \langle\beta(\mathbf{x})\rangle = \frac{1}{A_0}\int {\rm d}^2x\,\beta(\mathbf{x})$$

is the average of $\beta(\mathbf{x})$ over the whole interfacial area A_0. Substituting (16) in (31) and solving for J_0 gives an equation of the form (3) with $\alpha = \bar{\beta}$.

The first-order solution to (29) is

$$\psi(\mathbf{q}) = M\delta(\mathbf{q}) - \frac{M}{\kappa q}\beta(\mathbf{q})\left[1 - \frac{(2\pi)^2}{A_0}\delta(\mathbf{q})\right]. \quad (32)$$

Substituting (32) in (30) gives again an equation of the form (3) with

$$\alpha = \bar{\beta} - \frac{(2\pi)^2}{\kappa A_0}\int \mathrm{d}^2q \frac{1}{q}\langle|\beta(\mathbf{q})|^2\rangle\left[1 - \frac{(2\pi)^2}{A_0}\delta(\mathbf{q})\right], \quad (33)$$

where we have added $\langle\ldots\rangle$ which denotes ensemble average, and where we used that

$$\langle\beta(\mathbf{q})\beta(-\mathbf{q})\rangle = \langle|\beta(\mathbf{q})|^2\rangle.$$

We can rewrite (33) as follows. Let us define the correlation function

$$C_\beta(\mathbf{q}) = \frac{1}{(2\pi)^2}\int \mathrm{d}^2x\,\langle\beta(\mathbf{x})\beta(\mathbf{0})\rangle e^{i\mathbf{q}\cdot\mathbf{x}}. \quad (34)$$

Note that

$$C_\beta(\mathbf{q}) = \frac{(2\pi)^2}{A_0}\langle|\beta(\mathbf{q})|^2\rangle. \quad (35)$$

This equation follows from the fact that the statistical properties are assumed to be translational invariant in the $\mathbf{x}$-plane, and is proved as follows:

$$\begin{aligned} C_\beta(\mathbf{q}) &= \frac{1}{(2\pi)^2}\int \mathrm{d}^2x\,\langle\beta(\mathbf{x})\beta(\mathbf{0})\rangle e^{i\mathbf{q}\cdot\mathbf{x}} \\ &= \frac{1}{(2\pi)^2}\int \mathrm{d}^2x\,\langle\beta(\mathbf{x}+\mathbf{x}')\beta(\mathbf{x}')\rangle e^{i\mathbf{q}\cdot\mathbf{x}} \\ &= \frac{1}{(2\pi)^2}\int \mathrm{d}^2x''\,\langle\beta(\mathbf{x}'')\beta(\mathbf{x}')\rangle e^{i\mathbf{q}\cdot(\mathbf{x}''-\mathbf{x}')}. \end{aligned}$$

This equation must be independent of $\mathbf{x}'$ and we can therefore integrate over the $\mathbf{x}'$-plane and divide by the area A_0 giving

$$\begin{aligned} C_\beta(\mathbf{q}) &= \frac{1}{(2\pi)^2 A_0}\int \mathrm{d}^2x'\mathrm{d}^2x''\,\langle\beta(\mathbf{x}'')\beta(\mathbf{x}')\rangle e^{i\mathbf{q}\cdot(\mathbf{x}''-\mathbf{x}')} \\ &= \frac{(2\pi)^2}{A_0}\langle|\beta(\mathbf{q})|^2\rangle. \end{aligned}$$

Let us define

$$\Delta\beta(\mathbf{x}) = \beta(\mathbf{x}) - \bar{\beta}. \quad (36)$$

We get

$$\Delta\beta(\mathbf{q}) = \beta(\mathbf{q}) - \bar{\beta}\delta(\mathbf{q})$$

and thus

$$\langle|\Delta\beta(\mathbf{q})|^2\rangle = \langle|\beta(\mathbf{q})|^2\rangle\left[1 - \frac{(2\pi)^2}{A_0}\delta(\mathbf{q})\right], \quad (37)$$

where we have used that

$$\bar{\beta}\delta(\mathbf{q}) = \frac{(2\pi)^2}{A_0}\beta(\mathbf{q})\delta(\mathbf{q})$$

and that

$$\delta(\mathbf{q})\delta(-\mathbf{q}) = \delta(\mathbf{q})\frac{1}{(2\pi)^2}\int \mathrm{d}^2x\,e^{-i\mathbf{q}\cdot\mathbf{x}} = \delta(\mathbf{q})\frac{A_0}{(2\pi)^2}.$$

Using (33) and (37) gives

$$\alpha = \bar{\beta} - \frac{1}{\kappa}\int \mathrm{d}^2q q^{-1}C_{\Delta\beta}(\mathbf{q}). \quad (38)$$

Let us write

$$\langle\Delta\beta(\mathbf{x})\Delta\beta(\mathbf{0})\rangle = \langle(\Delta\beta)^2\rangle f(\mathbf{x}), \quad (39)$$

where $f(\mathbf{0}) = 1$. We write

$$f(\mathbf{x}) = \int \mathrm{d}^2q\, f(\mathbf{q})e^{i\mathbf{q}\cdot\mathbf{x}},$$

so that $f(\mathbf{x} = \mathbf{0}) = 1$ gives

$$\int \mathrm{d}^2q\, f(\mathbf{q}) = 1. \quad (40)$$

Using (39) and (40), eq. (38) takes the form

$$\alpha = \bar{\beta} - \langle(\Delta\beta)^2\rangle\kappa^{-1}l, \quad (41)$$

where the *correlation length*

$$l = \frac{\int \mathrm{d}^2q\, q^{-1}f(\mathbf{q})}{\int \mathrm{d}^2q\, f(\mathbf{q})}.$$

For randomly rough surfaces with isotropic statistical properties $f(\mathbf{q})$ depends only on $q = |\mathbf{q}|$ so that

$$l = \frac{\int_0^\infty \mathrm{d}q\, f(q)}{\int_0^\infty \mathrm{d}q\, qf(q)}.$$

Most surfaces of engineering interest are fractal-like, with the surface roughness power spectrum having a (long-distance) roll-off wave vector q_0. In this case one can show that $l \approx q_0^{-1}$. For the surface used in the numerical study presented below in sect. 4, one has $q_0 \approx 10^7\,\mathrm{m}^{-1}$ (see fig. 8). Furthermore, in this case (for amorphous silicon dioxide solids) $\kappa \approx 1\,\mathrm{W/mK}$ and if we assume that $\langle(\Delta\beta)^2\rangle$ is of order $\bar{\beta}^2$, we get the ratio between the second and the first term in (41) to be of order $\bar{\beta}/(q_0\kappa) \approx 0.01$, where we have used that typically (see fig. 9) $\bar{\beta} \approx 0.1\,\mathrm{MW/m^2K}$. Thus, in the application presented in sect. 4 the second term in the expansion (41) is negligible.

Equation (41) represents the first two terms in an infinite series which would result if (29) is iterated to infinite order. The result (41) is only useful if the first term $\bar{\beta}$ is much larger that the second term. If this is not the case one would need to include also higher-order terms (in principle, to infinite order) which becomes very hard to calculate using the iterative procedure. By comparing the magnitude between the two terms in (41), one can determine if it is legitimate to include only the lowest-order term $\bar{\beta}$.

We now consider two applications of (41), namely the contribution to the heat transfer from a) the electromagnetic field (in vacuum) and b) from heat transfer via a gas (*e.g.*, the normal atmosphere) which we assume is surrounding the two solids.

a) Radiative contribution to α (in vacuum)

The heat flux per unit area between two black-bodies separated by $d \gg d_T = c\hbar/k_{\rm B}T$ is given by the Stefan-Boltzmann law

$$J_0 = \frac{\pi^2 k_{\rm B}^4}{60\hbar^3 c^2}(T_0^4 - T_1^4),$$

where T_0 and T_1 are the temperatures of solids **1** and **2**, respectively, and c the light velocity. In this limiting case the heat transfer between the bodies is determined by the propagating electromagnetic waves radiated by the bodies and does not depend on the separation d between the bodies. Electromagnetic waves (or photons) always exist outside any body due to thermal or quantum fluctuations of the current density inside the body. The electromagnetic field created by the fluctuating current density exists also in the form of evanescent waves, which are damped exponentially with the distance away from the surface of the body. For an isolated body, the evanescent waves do not give a contribution to the energy radiation. However, for two solids separated by $d < d_T$, the heat transfer may increase by many orders of magnitude due to the evanescent electromagnetic waves —this is often referred to as photon tunneling.

For short separation between two solids with flat surfaces ($d \ll d_T$), the heat current due to the evanescent electromagnetic waves is given by [27]

$$J_0 = \frac{4}{(2\pi)^3}\int_0^\infty {\rm d}\omega\,(\Pi_0(\omega) - \Pi_1(\omega)) \times \int {\rm d}^2q\, e^{-2qd}\frac{{\rm Im}\, R_0(\omega)\,{\rm Im}\, R_1(\omega)}{|1 - e^{-2qd}R_0(\omega)R_1(\omega)|^2}\,, \qquad (42)$$

where

$$\Pi(\omega) = \hbar\omega\left(e^{\hbar\omega/k_{\rm B}T} - 1\right)^{-1}$$

and

$$R(\omega) = \frac{\epsilon(\omega) - 1}{\epsilon(\omega) + 1},$$

where $\epsilon(\omega)$ is the dielectric function. From (42) it follows that the heat current scales as $1/d^2$ with the separation between the solid surfaces. The heat current is especially large in the case of resonant photon tunneling between surface modes localized on the two different surfaces. The resonant condition corresponds to the case when the denominator in the integrand of (42) is small. Close to the resonance we can use the approximation

$$R \approx \frac{\omega_1}{\omega - \omega_0 - i\gamma}\,,$$

where ω_1 is a constant and ω_0 is determined by the equation ${\rm Re}[\epsilon(\omega_0) + 1] = 0$. In this case the heat current is determined by [27]

$$J_0 \approx \mu\frac{\gamma}{d^2}\left[\Pi_0(\omega_0) - \Pi_1(\omega_0)\right],$$

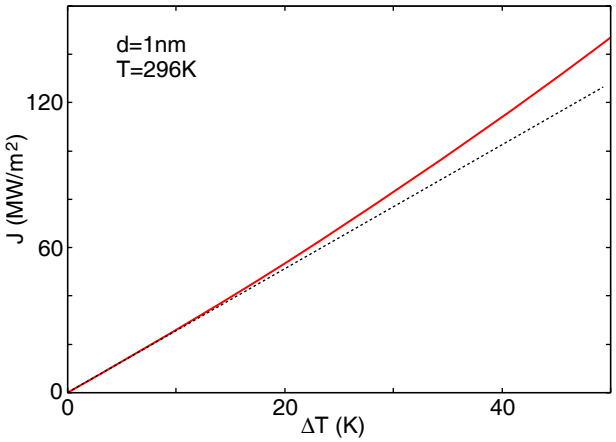

Fig. 4. Solid line: The calculated (using (42)) heat current per unit area, J_0, between two (amorphous) silicon dioxide bodies, as a function of the temperature difference ΔT. The solids have flat surfaces separated by $d = 1\,{\rm nm}$. One solid is at the temperature $T = 296\,{\rm K}$ and the other at $T + \Delta T$. Dashed line: linear function with the slope given by the initial slope (at $\Delta T = 0$) of the solid line.

where $\mu \approx [\log(2\omega_a/\gamma)]^2/(8\pi)$. If we write $T_1 = T_0 - \Delta T$ and assume $\Delta T/T_0 \ll 1$ we get $J_0 = \alpha\Delta T$, with

$$\alpha \approx \mu\frac{k_{\rm B}\gamma}{d^2}\frac{\eta^2\exp(\eta)}{[\exp(\eta) - 1]^2}\,, \qquad (43)$$

where $\eta = \hbar\omega_0/k_{\rm B}T_0$.

Resonant photon tunneling enhancement of the heat transfer is possible for two semiconductor or insulator surfaces which can support low-frequency surface phonon-polariton modes in the mid-infrared frequency region. As an example, consider two clean surfaces of (amorphous) silicon dioxide (SiO_2). The optical properties of this material can be described using an oscillator model [34]

$$\epsilon(\omega) = \epsilon_\infty + \frac{a}{\omega_a^2 - \omega^2 - i\omega\gamma_a} + \frac{b}{\omega_b^2 - \omega^2 - i\omega\gamma_b}\,.$$

The frequency-dependent term in this expression is due to optical phonons. The values for the parameters ϵ_∞, (a, ω_a, γ_a) and (b, ω_b, γ_b) are given in ref. [34]. In fig. 4 we show the calculated heat current per unit area, J_0, as a function of the temperature difference ΔT. The solids have flat surfaces separated by $d = 1\,{\rm nm}$. One solid is at the temperature $T = 296\,{\rm K}$ and the other at $T + \Delta T$. When $\Delta T \ll T$, the heat transfer depends (nearly) linearly on the temperature difference ΔT (see fig. 4), and we can define the heat transfer coefficient $\alpha = J_0/\Delta T$. In the present case (for $d = d_0 = 1\,{\rm nm}$) $\alpha = \alpha_0 \approx 2\times 10^6\,{\rm W/m^2K}$. If the surfaces are not smooth but if roughness occurs so that the separation d varies with the coordinate $\mathbf{x} = (x, y)$ we have to first order in the expansion (41)

$$\alpha = \bar\beta = \alpha_0\langle(d_0/d)^2\rangle, \qquad (44)$$

where $\langle\ldots\rangle$ stands for ensemble average, or average over the whole surface area, and where α_0 is the heat transfer between flat surfaces separated by $d = d_0$.

In the present case the heat transfer is associated with thermally excited optical (surface) phonons. That is, the electric field of a thermally excited optical phonon in one solid excites an optical phonon in the other solid, leading to energy transfer. The excitation transfer occurs in both directions but if one solid is hotter than the other, there will be a net transfer of energy from the hotter to the colder solid. For metals, low-energy excited electron-hole pairs will also contribute to the energy transfer, but for good metals the screening of the fluctuating electric field by the conduction electrons leads to very ineffective heat transfer. However, if the metals are covered with metal oxide layers, and if the separation between the solids is smaller than the oxide layer thickness, the energy transfer may again be due mainly to the optical phonons of the oxide, and the magnitude of the heat current will be similar to what we calculated above for (amorphous) silicon dioxide.

Let us consider a high-tech application. Consider a MEMS device involving very smooth (amorphous) silicon dioxide slabs. Consider, for example, a very thin silicon dioxide slab rotating on a silicon dioxide substrate. During operation a large amount of frictional energy may be generated at the interface. Assume that the disk is pressed against the substrate with the nominal stress or pressure p_0. This does not need to be an external applied force but may be due to the long-ranged van der Waals attraction between the solids, or due to capillary bridges formed in the vicinity of the (asperity) contact regions between the solids. The heat transfer due to the area of real contact (assuming purely elastic deformation) can be calculated from (25). Let us make a very rough estimate: Surfaces used in MEMS application have typically a roughness of order a few nanometers. Thus, $u_0 \sim 1\,\mathrm{nm}$ and for (amorphous) silicon dioxide the heat conductivity $\kappa \approx 1\,\mathrm{W/Km}$. Thus, from (26a)

$$\alpha \approx (p_0/E) \times 10^9\,\mathrm{W/m^2K}. \tag{45}$$

In a typical case the nominal pressure p_0 may be (due to the van der Waals interaction and capillary bridges) between 10^6 and $10^7\,\mathrm{Pa}$ and with $E \approx 10^{11}\,\mathrm{Pa}$ we get from (45) $\alpha \approx 10^4$–$10^5\,\mathrm{W/K\,m^2}$. If the root-mean-square roughness is of order $\sim 1\,\mathrm{nm}$, we expect the average separation between the surfaces to be of order a few nanometer so that $\langle (d_0/d)^2 \rangle \approx 0.1$ giving the non-contact contribution to α from the electromagnetic field of order (from (44)) $10^5\,\mathrm{W/K\,m^2}$, *i.e.*, larger than or of similar magnitude as the contribution from the area of real contact.

b) Contribution to α from heat transfer via the surrounding gas or liquid

Consider two solids with flat surfaces separated by a distance d. Assume that the solids are surrounded by a gas. Let Λ be the gas mean free path. If $d \gg \Lambda$ the heat transfer between the solids occurs via heat diffusion in the gas. If $d \ll \Lambda$ the heat transfer occurs by ballistic propagation of gas molecules from one surface to the other. In this case gas molecules reflected from the hotter surface will have (on the average) higher kinetic energy that the gas molecules reflected from the colder surface. This will result in heat transfer from the hotter to the colder surface. The heat current is approximately given by [35]

$$J_0 \approx \frac{\kappa_{\mathrm{gas}} \Delta T}{d + a\Lambda}\,,$$

where a is a number of order unity and which depends on the interaction between the gas molecules and the solid walls [2]. For air (and most other gases) at the normal atmospheric pressure and at room temperature $\Lambda \approx 65\,\mathrm{nm}$ and $\kappa_{\mathrm{gas}} \approx 0.02\,\mathrm{W/m\,K}$. For contacting surfaces with surface roughness we get, to first order in the expansion in (41),

$$\alpha \approx \kappa_{\mathrm{gas}} \langle (d + \Lambda)^{-1} \rangle = \kappa_{\mathrm{gas}} \int_0^\infty \mathrm{d}u\, P(u)(u + \Lambda)^{-1}, \tag{46}$$

where $\langle \ldots \rangle$ stands for ensemble average or averaging over the surface area, and where $P(u)$ is the probability distribution of interfacial separations. Equation (46) also holds if the surfaces are surrounded by a liquid rather than a gas. In this case κ_{gas} must be replaced with the liquid heat conductivity κ_{liq} and in most cases one can put Λ equal to zero.

If we again consider a MEMS application where the average surface separation is of order nm, we can neglect the d-dependence in (46) and get $\alpha \approx \kappa_{\mathrm{gas}}/\Lambda \approx 3 \times 10^5\,\mathrm{W/m^2K}$ which is similar to the contribution from the electromagnetic coupling.

c) Contribution to α from heat transfer via capillary bridges

If the solid walls are wet by water, in a humid atmosphere capillary bridges will form spontaneously at the interface in the vicinity of the asperity contact regions. For very smooth surfaces, such as in MEMS applications, the fluid (in this case water) may occupy a large region between the surfaces and will then dominate the heat transfer between the solids. Similarly, contamination layers (mainly organic molecules) which cover most natural surfaces may form capillary bridges between the contacting solids, and contribute in an important way to the heat transfer coefficient. The fraction of the interfacial surface area occupied by fluid bridges, and the separation between the solids in the fluid-covered region, can be calculated using the theory developed in ref. [36]. From this one can calculate the contribution to the heat transfer using (46),

$$\alpha \approx \kappa_{\mathrm{liq}} \langle d^{-1} \rangle \approx \kappa_{\mathrm{liq}} \int_a^{d_{\mathrm{K}}} \mathrm{d}u\, P(u) u^{-1}, \tag{47}$$

where $P(u)$ is the distribution of interfacial separation u, and A_0 the nominal contact area. The lower cut-off a in the integral is a distance of order a molecular length and d_{K} is the maximum height of the liquid bridge which, for a system in thermal equilibrium and for a wetting liquid, is of order the Kelvin length. Note that $P(u)$ is normalized and that

$$\int_a^{d_{\mathrm{K}}} \mathrm{d}u A_0 P(u) = \Delta A \tag{48}$$

is the surface area (projected on the xy-plane) where the surface separation is between $a < u < d_{\mathrm{K}}$.

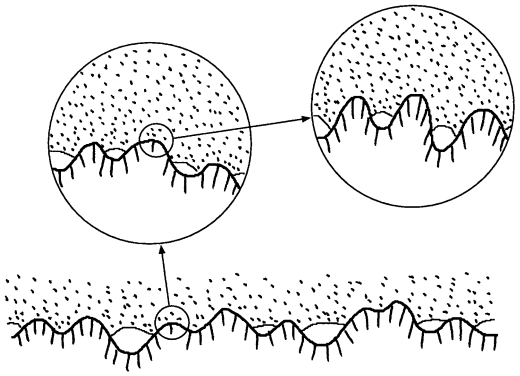

Fig. 5. A rubber block (dotted area) in adhesive contact with a hard rough substrate (hatched area). The substrate has roughness on many different length scales and the rubber makes partial contact with the substrate on all length scales. When a contact area is studied at low magnification it appears as if complete contact occurs, but when the magnification is increased it is observed that in reality only partial contact occurs.

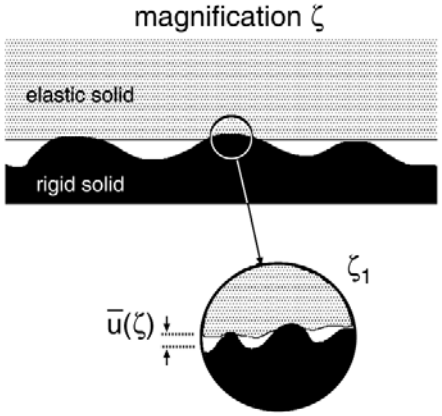

Fig. 6. An asperity contact region observed at magnification ζ. It appears that complete contact occurs in the asperity contact region, but when the magnification is increasing to the highest (atomic scale) magnification ζ_1, it is observed that the solids are actually separated by the average distance $\bar{u}(\zeta)$.

3 Contact mechanics: short review and basic equations

The theory of heat transfer presented above depends on quantities which can be calculated using contact mechanics theories. Thus, the heat flux through the non-contact area (sect. 2.2.2) depends on the average of some function $f[d(\mathbf{x})]$ of the interfacial separation $d(\mathbf{x})$. If $P(u)$ denotes the probability distribution of interfacial separation u, then

$$\langle f(d)\rangle = \int_a^\infty \mathrm{d}u\, f(u)P(u), \tag{49}$$

where a is a short-distance cut-off (typically of molecular dimension). The contribution from the area of real contact depends on the elastic energy $U_{\rm el}$ stored in the asperity contact regions (see eq. (23)). In the limit of small contact pressure $U_{\rm el} = p_0 u_0$, where u_0 is a length which is of order the root-mean-square roughness of the combined roughness profile. All the quantities $P(u)$, $U_{\rm el}$ and u_0 can be calculated with good accuracy using the contact mechanics model of Persson. Here we will briefly review this theory and give the basic equations relevant for heat transfer.

Consider the frictionless contact between two elastic solids with Young's elastic modulus E_0 and E_1 and the Poisson ratios ν_0 and ν_1. Assume that the solid surfaces have height profiles $h_0(\mathbf{x})$ and $h_1(\mathbf{x})$, respectively. The elastic contact mechanics for the solids is equivalent to those of a rigid substrate with the height profile $h(\mathbf{x}) = h_0(\mathbf{x}) + h_1(\mathbf{x})$ and a second elastic solid with a flat surface and with Young's modulus E and Poisson ratio ν chosen so that [37]

$$\frac{1-\nu^2}{E} = \frac{1-\nu_0^2}{E_0} + \frac{1-\nu_1^2}{E_1}\,. \tag{50}$$

The contact mechanics formalism developed elsewhere [10–14] is based on studying the interface between two contacting solids at different magnification ζ, see fig. 5. When the system is studied at the magnification ζ it appears as if the contact area (projected on the xy-plane) equals $A(\zeta)$, but when the magnification increases it is observed that the contact is incomplete, and the surfaces in the apparent contact area $A(\zeta)$ are in fact separated by the average distance $\bar{u}(\zeta)$, see fig. 6. The (apparent) relative contact area $A(\zeta)/A_0$ at the magnification ζ is given by [10–13]

$$\frac{A(\zeta)}{A_0} = \frac{1}{(\pi G)^{1/2}} \int_0^{p_0} \mathrm{d}\sigma\, \mathrm{e}^{-\sigma^2/4G} = \mathrm{erf}\left(\frac{p_0}{2G^{1/2}}\right), \tag{51}$$

where

$$G(\zeta) = \frac{\pi}{4}\left(\frac{E}{1-\nu^2}\right)^2 \int_{q_0}^{\zeta q_0} \mathrm{d}q q^3 C(q), \tag{52}$$

where the surface roughness power spectrum

$$C(q) = \frac{1}{(2\pi)^2}\int \mathrm{d}^2x\, \langle h(\mathbf{x})h(\mathbf{0})\rangle \mathrm{e}^{-i\mathbf{q}\cdot\mathbf{x}}, \tag{53}$$

where $\langle \ldots \rangle$ stands for ensemble average. The height profile $h(\mathbf{x})$ of the rough surface can be measured routinely today on all relevant length scales using optical and stylus experiments.

We define $u_1(\zeta)$ to be the (average) height separating the surfaces which appear to come into contact when the magnification decreases from ζ to $\zeta - \Delta\zeta$, where $\Delta\zeta$ is a small (infinitesimal) change in the magnification. $u_1(\zeta)$ is a monotonically decreasing function of ζ, and can be calculated from the average interfacial separation $\bar{u}(\zeta)$ and $A(\zeta)$ using (see ref. [13])

$$u_1(\zeta) = \bar{u}(\zeta) + \bar{u}'(\zeta)A(\zeta)/A'(\zeta), \tag{54}$$

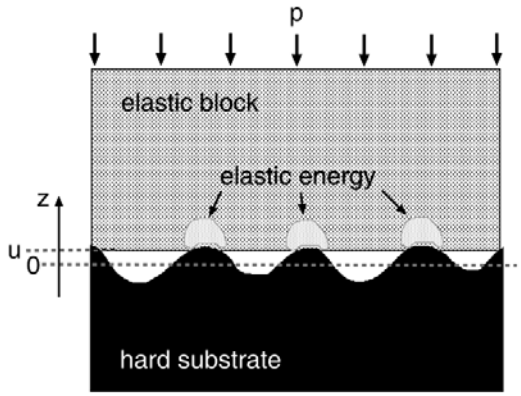

Fig. 7. An elastic block squeezed against a rigid rough substrate. The separation between the average plane of the substrate and the average plane of the lower surface of the block is denoted by u. Elastic energy is stored in the block in the vicinity of the asperity contact regions.

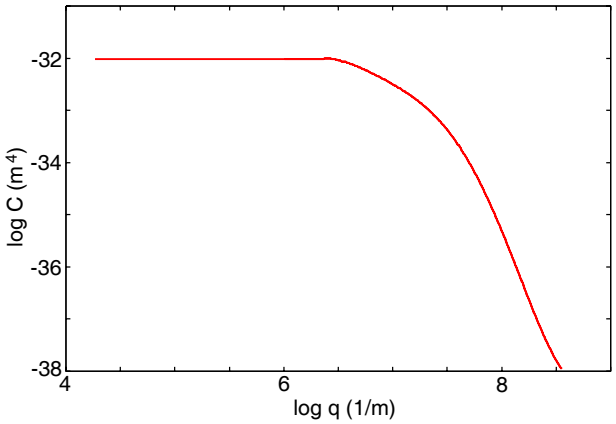

Fig. 8. Surface roughness power spectrum $C(q)$ as a function of the wave vector q on a log-log scale (with 10 as basis). For a typical surface used in MEMS applications with the root-mean-square roughness 2.5 nm when measured over an area of $10\,\mu\text{m} \times 10\,\mu\text{m}$.

where [13]

$$\bar{u}(\zeta) = \sqrt{\pi}\int_{\zeta q_0}^{q_1} \mathrm{d}q\, q^2 C(q) w(q) \times \int_{p(\zeta)}^{\infty} \mathrm{d}p'\, \frac{1}{p'} e^{-[w(q,\zeta)p'/E^*]^2}, \quad (55)$$

where $E^* = E/(1-\nu^2)$, and where $p(\zeta) = p_0 A_0/A(\zeta)$ and

$$w(q,\zeta) = \left(\pi \int_{\zeta q_0}^{q} \mathrm{d}q'\, q'^3 C(q')\right)^{-1/2}.$$

The distribution of interfacial separations

$$P(u) = \langle \delta[u - u(\mathbf{x})]\rangle,$$

where $u(\mathbf{x}) = d(\mathbf{x})$ is the separation between the surfaces at point $\mathbf{x}$. As shown in ref. [13] we have (approximately)

$$P(u) = \int_1^{\infty} \mathrm{d}\zeta\, [-A'(\zeta)]\delta[u - u_1(\zeta)]. \quad (56a)$$

Thus we can write (49) as

$$\langle f(d)\rangle = \int_1^{\zeta_1} \mathrm{d}\zeta\, [-A'(\zeta)] f[u_1(\zeta)], \quad (56b)$$

where ζ_1 is defined by $u_1(\zeta_1) = a$.

Finally, the elastic energy $U_{\rm el}$ (see fig. 7) and the length parameter u_0 can be calculated as follows. The elastic energy $U_{\rm el}$ has been studied in ref. [8]:

$$U_{\rm el} = A_0 E^* \frac{\pi}{2} \int_{q_0}^{q_1} \mathrm{d}q\, q^2 W(q,p) C(q). \quad (57)$$

In the simplest case one takes, $W(q,p) = P(q,p) = A(\zeta)/A_0$ is the relative contact area when the interface is studied at the magnification $\zeta = q/q_0$, which depends on the applied pressure $p = p_0$. A more accurate expression is

$$W(q,p) = P(q,p)[\gamma + (1-\gamma)P^2(q,p)]. \quad (58)$$

However, in this case one also need to modify (55) appropriately (see ref. [13]). The parameter γ in (58) seems to depend on the surface roughness. For self-affine fractal surfaces with the fractal dimension $D_{\rm f} \approx 2.2$ we have found that $\gamma \approx 0.5$ gives a good agreement between the theory and numerical studies [15]. As $D_{\rm f} \to 2$, the analysis of numerical data indicates that $\gamma \to 1$.

For small pressures one can show that [13]

$$p = \beta E^* e^{-\bar{u}/u_0}, \quad (59)$$

where

$$u_0 = \sqrt{\pi}\gamma \int_{q_0}^{q_1} \mathrm{d}q\, q^2 C(q) w(q), \quad (60)$$

where $w(q) = w(q,1)$, and where

$$\beta = \epsilon \exp\left[\frac{\int_{q_0}^{q_1} \mathrm{d}q\, q^2 C(q) w(q) \log w(q)}{\int_{q_0}^{q_1} \mathrm{d}q\, q^2 C(q) w(q)}\right], \quad (61)$$

where (for $\gamma = 1$) $\epsilon = 0.7493$.

4 Numerical results

In this section we present numerical results to illustrate the theory. We focus on a MEMS-like application. In fig. 8 we show the surface roughness power spectrum $C(q)$ as a function of the wave vector q on a log-log scale (with 10 as basis) for a typical surface used in MEMS applications, with the root-mean-square roughness 2.5 nm when measured over an area $10\,\mu\text{m} \times 10\,\mu\text{m}$. In fig. 9 we show for this case the contribution to the heat transfer coefficient α from the direct contact area, and the non-contact

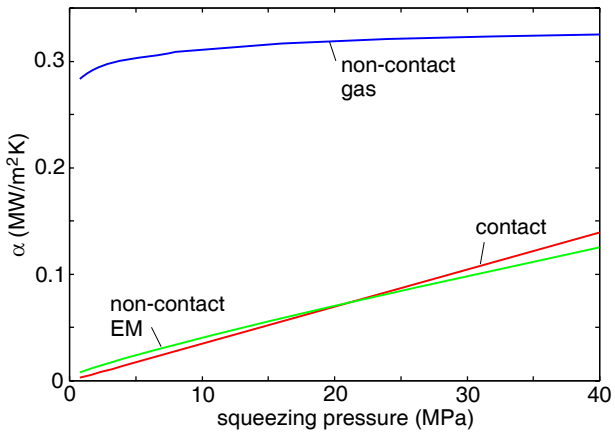

Fig. 9. The contribution to the heat transfer coefficient α from the direct contact area, and the non-contact contribution due to the fluctuating electromagnetic (EM) field and due to heat transfer via the surrounding gas. For a randomly rough surface with the (combined) surface roughness power spectrum shown in fig. 8.

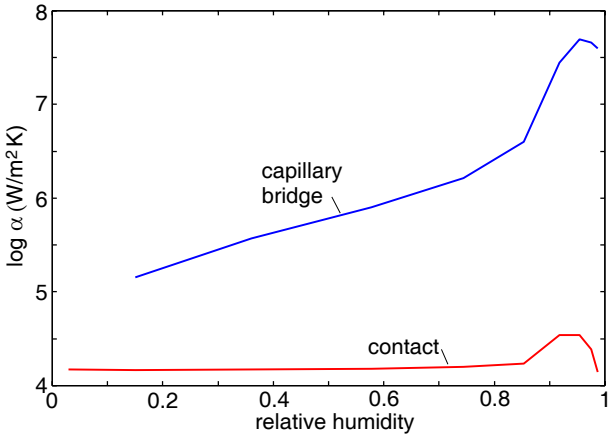

Fig. 10. The logarithm (with 10 as basis) of the contribution to the heat transfer coefficient α from the real contact area, and from the water in the capillary bridges, as a function of the relative (water) humidity. For a randomly rough surface with the (combined) surface roughness power spectrum shown in fig. 8. The squeezing pressure $p_0 = 4\,\mathrm{MPa}$ and the effective elastic modulus $E^* = 86\,\mathrm{GPa}$. The heat conductivity of water $\kappa_{\mathrm{fluid}} = 0.58\,\mathrm{W/m\,K}$.

contribution due to the fluctuating electromagnetic (EM) field and due to heat transfer via the surrounding gas. In the calculation of the EM-contribution we have used (44), with $\alpha_0 = 2.0\,\mathrm{MW/m^2K}$ (and $d_0 = 1\,\mathrm{nm}$). For the contribution from the surrounding gas we have used (46), with $\kappa_{\mathrm{gas}} = 0.024\,\mathrm{W/m\,K}$ and $\Lambda = 65\,\mathrm{nm}$ (and $a = 1$). For the contact contribution we used (25) with $\kappa = 1\,\mathrm{W/m\,K}$. In all calculations we have assumed $E^* = 86\,\mathrm{GPa}$ and that the contact is elastic (no plastic yielding). The relative weak (squeezing) pressure dependence of the contribution from the non-contact area is due to the fact that the (average) surface separation is smaller than the mean free path Λ of the gas molecules in the non-contact area. Thus, for squeezing pressures above $\sim 100\,\mathrm{MPa}$ the contact contribution will dominate the heat transfer.

We have also studied the contribution to the heat transfer from capillary bridges which on hydrophilic surfaces form spontaneously in a humid atmosphere. The capillary bridges give an attractive force (to be added to the external squeezing force), which pulls the solids closer together. We have used the theory presented in ref. [36] to include the influence of capillary bridges on the contact mechanics, and to determine the fraction of the interface area filled with fluid at any given relative humidity. In fig. 10 we show the logarithm (with 10 as basis) of the contribution to the heat transfer coefficient α from the real contact areas, and from the water in the capillary bridges, as a function of the relative (water) humidity. For relative humidity below ~ 0.4 the contribution to the heat transfer from capillary bridges decreases roughly linearly with decreasing humidity (and vanishes at zero humidity), and for relative humidity below ~ 0.015 the heat transfer via the area of real contact will be more important than the contribution from the capillary bridges. However the contribution from heat transfer via the air or vapor phase (not shown) is about $\sim 0.3\,\mathrm{MW/m^2K}$ (see fig. 9), and will hence give the dominant contribution to the heat transfer for relative humidity below 0.3. The small increase in the contribution from the area of real contact for relative humidity around ~ 0.94 is due to the increase in the contact area due to the force from the capillary bridges. For soft elastic solids (such as rubber) this effect is much more important: see ref. [36] for a detailed discussion of this effect, which will also affect (increase) the heat transfer in a drastic way.

We note that heat transfer via capillary bridges has recently been observed in nanoscale point contact experiments [38]. In this study the authors investigated the heat transfer mechanisms at a $\sim 100\,\mathrm{nm}$ diameter point contact between a sample and a probe tip of a scanning thermal microscope. They observed heat transfer both due to the surrounding (atmospheric) air, and via capillary bridges.

5 Role of adhesion and plastic deformation

In the theory above we have assumed that the solids deform purely elastically. However, in many practical situations the solids will deform plastically at short enough length scale. Similarly, in many practical situations, in particular for elastically soft solids, the area of real contact may depend strongly on the adhesive interaction across the contacting interface. Here we will briefly discuss under which circumstances this will affect the heat transfer between the solids.

The contribution to the heat transfer from the area of real contact between two solids depends on the elastic energy U_{el} stored in the asperity contact regions, or, at small enough applied loads, on the length parameter u_0. For most randomly rough surfaces these quantities are determined mainly by the long-wavelength, large-amplitude surface roughness components. Similarly, the interfacial separation, which determines the non-contact

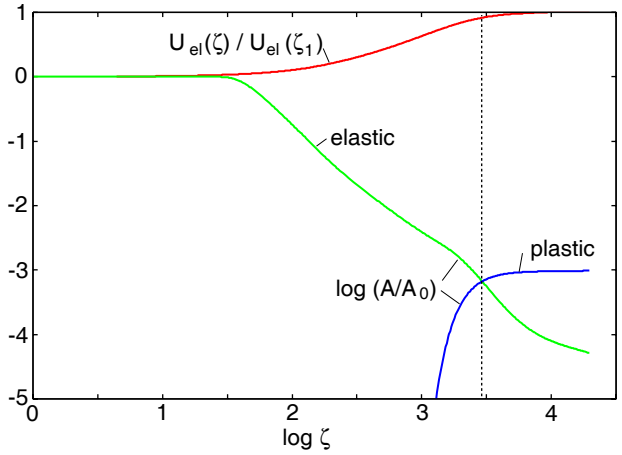

Fig. 11. The elastic $A_{\rm el}$ and plastic $A_{\rm pl}$ contact area as a function of magnification on a log-log scale (with 10 as basis). The penetration hardness $\sigma_{\rm Y} = 4\,{\rm GPa}$ and the applied pressure $p_0 = 4\,{\rm MPa}$. Also shown is the asperity-induced elastic energy $U_{\rm el}(\zeta)$ in units of the full elastic energy $U_{\rm el}(\zeta_1)$ obtained when all the roughness (with wave vectors below $q_1 = \zeta_1 q_0$) is included. The vertical dashed line indicate the magnification where $A_{\rm el} = A_{\rm pl}$.

contribution to the heat transfer, depends mainly on the long-wavelength, large amplitude surface roughness components. On the other hand, plastic deformation and adhesion often manifest themself only at short length scales, corresponding to high magnification. For this reason, in many cases one may assume purely elastic deformation when calculating the heat transfer, even if, at short enough length scale, all asperities have yielded plastically, or the adhesion has strongly increased the (apparent) contact area. Let us illustrate this with the amorphous silicon dioxide system studied in sect. 4.

In fig. 11 we show the elastic and plastic contact area as a function of magnification on a log-log scale (with 10 as basis). Also shown is the asperity-induced elastic energy $U_{\rm el}(\zeta)$ in units of the full elastic energy $U_{\rm el}(\zeta_1)$ obtained when all the roughness (with wave vectors below $q_1 = \zeta_1 q_0$) is included. Note that about 90% of the full elastic energy is already obtained at the magnification where the elastic and plastic contact areas are equal, and about 60% of the full elastic energy is obtained when $A_{\rm pl}/A_{\rm el} \approx 0.01$. Thus, in the present case, to a good approximation, we can neglect the plastic deformation when studying the heat transfer. In the calculation we have assumed the penetration hardness $\sigma_{\rm Y} = 4\,{\rm GPa}$ and the squeezing pressure $p_0 = 4\,{\rm MPa}$. Thus, at high magnification, where all the contact regions are plastically deformed, the relative contact area $A/A_0 = p_0/\sigma_{\rm Y} = 0.001$, which is in good agreement with the numerical data in fig. 11.

If necessary, it is easy to include adhesion and plastic deformation when calculating the heat transfer coefficient α. Thus (26b) is also valid when adhesion is included, at least as long as adhesion is treated as a contact interaction. However, in this case the interfacial stiffness ${\rm d}p_0/{\rm d}\bar{u}$ must be calculated including the adhesion (see ref. [39]). Plastic deformation can be included in an approximate way as follows. If two solids are squeezed together at the pressure p_0 they will deform elastically and, at short enough length scale, plastically. If the contact is now removed the surfaces will be locally plastically deformed. Assume now that the surfaces are moved into contact again at exactly the same position as the original contact, and with the same squeezing pressure p_0 applied. In this case the solids will deform purely elastically and the theory outlined in this paper can be (approximately) applied assuming that the surface roughness power spectrum $\bar{C}(q)$ of the (plastically) deformed surface is known. In ref. [14] we have described an approximately way of how to obtain $\bar{C}(q)$ from $C(q)$ by defining (with $q = \zeta q_0$) [40]

$$\bar{C}(q) = \left[1 - \left(\frac{A_{\rm pl}(\zeta)}{A_{\rm pl}^0}\right)^6\right] C(q),$$

where $A_{\rm pl}^0 = F_{\rm N}/\sigma_{\rm Y}$. The basic picture behind this definition is that surface roughness at short length scales gets smoothed out by plastic deformation, resulting in an effective cut-off of the power spectrum for large wave vectors (corresponding to short distances).

6 Application to tires

Here we will briefly discuss heat transfer in the context of tires. The rolling resistance $\mu_{\rm R}$ of a tire determines the heat production in a tire during driving on a strait planar road at a constant velocity v. In a stationary state the energy produced per unit time, $W = \mu_{\rm R} F_{\rm N} v$, must equal the transfer of energy per unit time, from the tire to the surrounding atmosphere and to the road surface. Here we will briefly discuss the relative importance of these two different contributions to the heat transfer.

Assume for simplicity that the frictional heat is produced uniformly in the tread rubber, and assume a tire without tread pattern. Let z be a coordinate axis perpendicular to the rubber surface. In this case at stationary condition the temperature in the tread rubber satisfies $T''(z) = -\dot{q}/\kappa$, where $\dot{q}$ is the frictional heat produced per unit volume and unit time. We assume that the heat current vanish at the inner rubber surface ($z = 0$, see fig. 12), so that $T'(0) = 0$. Thus we get $T(z) = T_0 - \dot{q}z^2/2\kappa$. The heat current at the outer rubber surface is

$$J_0 = -\kappa T'(d) = \dot{q}d. \tag{62}$$

The temperature of the outer surface of the tread rubber

$$T_1 = T(d) = T_0 - \dot{q}d^2/2\kappa. \tag{63}$$

Let us now assume that the heat transfer to the surrounding medium is

$$J_0 = \alpha(T_1 - T_{\rm air}). \tag{64}$$

Combining (62)–(64) gives

$$T_1 = T_0 - \frac{T_0 - T_{\rm air}}{1 + 2\kappa/d\alpha}\,. \tag{65}$$

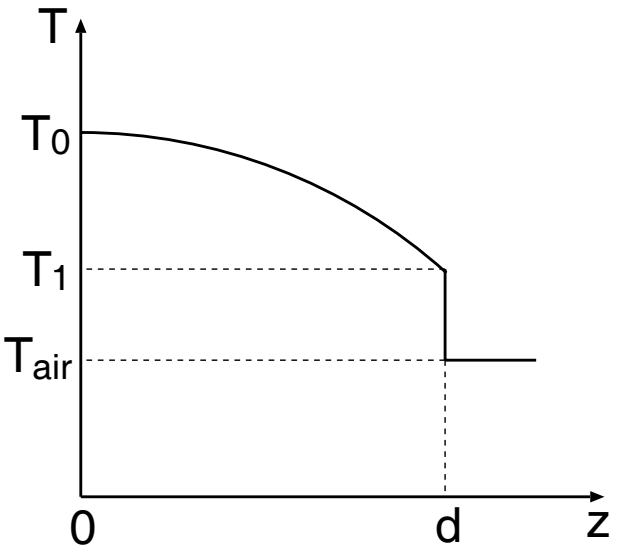

Fig. 12. Temperature distribution of rubber tread (thickness d) in contact with the air. The air temperature (for $z > d$) and the temperature at the outer ($z = d$) and inner ($z = 0$) rubber surfaces are denoted by $T_{\rm air}$, T_1 and T_0, respectively.

For rubber $\kappa \approx 0.2\,{\rm W/m\,K}$ and with $d = 1\,{\rm cm}$ and $\alpha \approx 100\,{\rm W/m^2K}$, as is typical for (forced) convective heat transfer between a tire and (dry) air (see Appendix D and ref. [41]), we get

$$T_1 \approx 0.3T_0 + 0.7T_{\rm air}.$$

The temperature profile is shown (schematically) in fig. 12. Actually, the heat production, even during pure rolling, will be somewhat larger close to the outer surface of the tread and the resulting temperature profile in the tread rubber will therefore be more uniform than indicated by the analysis above.

Let us now discuss the relative importance of the contributions to the heat transfer to the air and to the road. We assume that the heat transfer to the atmosphere and to the road are proportional to the temperature difference $T_1 - T_{\rm air}$ and $T_1 - T_{\rm road}$, respectively. We get

$$\mu_{\rm R} F_{\rm N} v = \alpha_{\rm air} A_{\rm surf}(T_1 - T_{\rm air}) + \alpha_{\rm road} A_0 (T_1 - T_{\rm road}), \quad (66)$$

where $A_{\rm surf}$ is the outer surface area of the tread, and A_0 the nominal tire-road footprint area. For rubber in contact with a road surface, κ in eq. (26) is $\approx 0.2\,{\rm W/m\,K}$ and with $p_0/E^* \approx 0.04$ and $u_0 \approx 10^{-3}\,{\rm m}$ (as calculated for a typical case) we get $\alpha_{\rm road} \approx 10\,{\rm W/m^2K}$ which is smaller than the contribution from the forced convection. Since the nominal contact area between the tire and the road is much smaller than the total rubber tread area, we conclude that the contribution from the area of real contact between the road and the tire is rather unimportant. During fast acceleration wear process may occur, involving the transfer of hot rubber particles to the road surface, but such processes will not be considered here. In addition, at the inlet of the tire-road footprint area, air may be compressed and then rapidly squeezed out from the tire-road contact area resulting in strong forced convective cooling of the rubber surface in the contact area. A similar process involving the inflow of air occurs at the exit of the tire-road footprint area. A detailed study of this complex process is necessary in order to accurately determine the heat transfer from a tire to the surrounding atmosphere and the road surface.

For a passenger car tire during driving on a strait planar road at a constant velocity v, the tire temperature which follows from (66) is in reasonable agreement with experiment. Thus, using (66), we get

$$\Delta T = T_1 - T_{\rm air} \approx \frac{\mu_{\rm R} F_{\rm N} v}{\alpha_{\rm air} A_{\rm surf}}, \quad (67)$$

and with $\alpha_{\rm air} = 100\,{\rm W/m^2K}$, $A_{\rm surf} \approx 0.5\,{\rm m^2}$ and $\mu_{\rm R} \approx 0.02$, $F_{\rm N} = 3500\,{\rm N}$ and $v = 30\,{\rm m/s}$, we get $\Delta T \approx 40\,^\circ{\rm C}$.

The discussion above has focused on the stationary state where the heat energy produced in the tire per unit time is equal to the energy given off to the surrounding per unit time. However, for a rolling tire it may take a very long time to arrive at this stationary state. In the simplest picture, assuming a uniform temperature in the tire rubber, we get from energy conservation

$$\rho C_V \frac{{\rm d}T}{{\rm d}t} = \dot{q} - \frac{\alpha}{d}(T - T_{\rm air}),$$

or, if $T(0) = T_{\rm air}$,

$$T(t) = T_{\rm air} + \frac{\dot{q} d}{\alpha}\left(1 - e^{-t/\tau}\right),$$

where the relaxation time $\tau = \rho C_V d/\alpha \approx 200\,{\rm s}$. In reality, the temperature in the tire is not uniform, and this will introduce another relaxation time τ', defined as the time it takes for heat to diffuse a distance d, which is of order $\tau' = \rho C_V d^2/\kappa$. The ratio $\tau'/\tau = \alpha d/\kappa$. For rubber $\kappa \approx 0.2\,{\rm W/m\,K}$ and assuming $d = 1\,{\rm cm}$ and $\alpha = 100\,{\rm W/m^2K}$ gives $\tau'/\tau \approx 5$ or $\tau' \approx 10^3\,{\rm s}$. Experiment have shown that it typically takes ~ 30 minutes to fully build up the tire temperature during rolling [41].

Rubber friction depends sensitively on the temperature of the rubber, in particular the temperature close to the rubber surface in contact with the road. The temperature in the surface region of a tire varies rapidly in space and time, which must be considered when calculating the rubber friction [1]. The shortest time and length scales are related to the contact between the road asperities and the rubber surface in the tire-road footprint contact area. During slip this generates intense heating which varies over length scales from a few micrometer to several mm, and over time scales shorter than the time a rubber patch stays in the footprint, which typically may be of order a few milliseconds. During this short time, very little heat is transferred to the surrounding, and very little heat conduction occurs inside the rubber, *i.e.*, the heat energy mainly stays where it is produced by the internal friction in the rubber. This results in a *flash temperature* effect, which has a crucial influence on rubber friction [1]. However, rubber friction also depends on the *background temperature* (usually denoted by T_0), which varies relatively slowly in space and time, *e.g.*, on time scales from

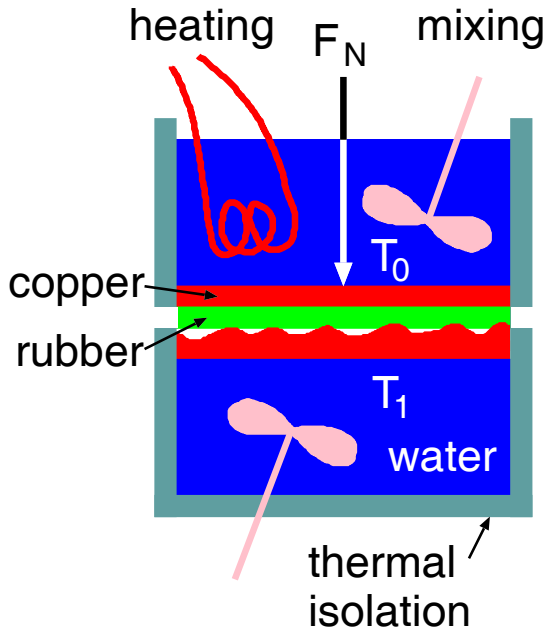

Fig. 13. Experiment to test the theory predictions for the heat transfer across interfaces. The increase in the temperature $T_1(t)$ of the water in the lower container, with increasing time t, determines the heat transfer between the upper and lower water container.

the time $\sim 0.1\,\mathrm{s}$ it takes for the tire to perform a few rotations, up to the time ~ 30 minutes necessary to build up the full tire temperature after any change in the driving condition (*e.g.*, from the start of driving). Note that the time variation of the background temperature T_0 depends on the surrounding (*e.g.*, the air and road temperatures, humidity, rain, ...) and on the driving history, while the flash temperature effect mainly depends on the slip history of a tread block (or rubber surface patch) in the footprint contact area, but not on the outside air or road temperature, or atmospheric condition.

7 A new experiment

We have performed a very simple experiment to test the theoretical predictions for the heat transfer. The setup is shown in fig. 13 and consists of two containers, both filled with distilled water, standing on top of each other with a thin silicon rubber film in between. The upper container is made from copper (inner diameter 5 cm), and the water is heated to the boiling temperature (*i.e.*, $T_0 = 100\,^\circ\mathrm{C}$). The lower container is made from PMMA with a cylindrical copper block at the top. To study the effect of surface roughness on the heat transfer, the copper block can be replaced with another copper block with different surface roughness. In the experiments presented below we used 3 copper blocks with different surface roughness.

The temperature $T_1(t)$ of the water in the lower container will increase with time t due to the heat current J_0 flowing from the upper container to the lower container:

$$J_0 = \rho C_V \dot{T}_1 d, \tag{68}$$

where d is the height of the water column in the lower container (in our experiment $d = 3.5\,\mathrm{cm}$), and where ρ and C_V are the water mass density and heat capacity, respectively. We measure the temperature of the water in the lower container as a function of time, starting at $25\,^\circ\mathrm{C}$. To obtain a uniform temperature of the water in the lower container, we mix it using a (magnetic-driven) rotating metal bar.

We have investigated the heat transfer using copper blocks with different surface roughness. To prepare the rough surfaces, we have pressed annealed (plastically soft) copper blocks with smooth surface against sandpaper, using a hydraulic press. We repeated this procedure several times to obtain randomly rough surfaces. The roughness of the copper surfaces can be changed by using sandpaper of different grade (consisting of particles with different (average) diameter). Due to the surface roughness, the contact between the top surface of the lower container and the thin silicon rubber sheet (thickness $d_0 = 2.5\,\mathrm{mm}$) attached to the upper container, is only partial. The bottom surface of the upper container has been highly polished and we can neglect the heat resistance at this rubber-copper interface. Thus, most of the resistance to the heat flow arises from the heat diffusion through the rubber sheet, and from the resistance to the heat flow at the interface between the rubber and the rough copper block.

The rubber sheet (elastic modulus $E = 2.5\,\mathrm{MPa}$, Poisson ratio $\nu = 0.5$) was made from a silicone elastomer (PDMS). We have used Polydimethylsiloxane because of its almost purely elastic behavior on the time scales involved in our experiments. The PDMS sample was prepared using a two-component kit (Sylgard 184) purchased from Dow Corning (Midland, MI). This kit consists of a base (vinyl-terminated polydimethylsiloxane) and a curing agent (methylhydrosiloxane-dimethylsiloxane copolymer) with a suitable catalyst. From these two components we prepared a mixture of 10:1 (base/cross linker) in weight. The mixture was degassed to remove the trapped air induced by stirring from the mixing process and then poured into cylindrical casts (diameter 5 cm and height $d_0 = 2.5\,\mathrm{mm}$). The bottom of these casts were made from glass to obtain smooth surfaces (negligible roughness). The samples were cured in an oven at $80\,^\circ\mathrm{C}$ for over 12 hours.

Using (3), we can write

$$J_0 \approx \frac{T_0 - T_1(t)}{d_0\kappa_0^{-1} + \alpha^{-1}}\,, \tag{69}$$

where κ_0 is the heat conductivity of the rubber. Here we have neglected the influence of the copper blocks on the heat transfer resistance, which is a good approximation because of the high thermal conductivity of copper. Combining (68) and (69) gives

$$\tau_0 \dot{T}_1 = T_0 - T_1(t),$$

where the relaxation time is

$$\tau_0 = \rho C_V d \left(\frac{d_0}{\kappa_0} + \frac{1}{\alpha} \right).$$

If we assume that τ_0 is time independent, we get

$$T_1(t) = T_0 + [T_1(0) - T_0] e^{-t/\tau_0}. \qquad (70a)$$

In the study above we have assumed that there is no heat transfer from the lower container to the surrounding. However, if necessary one can easily take into account such a heat transfer: If we assume that the heat transfer depends linearly on the temperature difference between the water and the surrounding we can write

$$J_1 = \alpha_1 (T_1 - T_{\rm surr}).$$

In this case it is easy to show that (70a) is replaced with

$$T_1(t) = T_a + [T_1(0) - T_a] e^{-t/\tau}, \qquad (70b)$$

where T_a is the temperature in the water after a long time (stationary state where $J_0 = J_1$), and where the relaxation time τ now is given by

$$\tau = \rho C_V d \frac{T_a - T_{\rm surr}}{T_0 - T_{\rm surr}} \left(\frac{d_0}{\kappa_0} + \frac{1}{\alpha} \right).$$

The heat transfer across the rubber-copper interface can occur via the area of real contact, or via the non-contact area via heat diffusion in the thin air film or via radiative heat transfer. Since all these heat transfer processes act in parallel, we have

$$\alpha \approx \alpha_{\rm gas} + \alpha_{\rm con} + \alpha_{\rm rad}.$$

Let us estimate the relative importance of these different contributions to α. Using the (diffusive) heat conductivity of air $\kappa_{\rm gas} \approx 0.02\,{\rm W/m\,K}$ and assuming $\langle d^{-1} \rangle = (20\,\mu{\rm m})^{-1}$ gives

$$\alpha_{\rm gas} = \kappa_{\rm gas} \langle (d + \Lambda)^{-1} \rangle \approx \kappa_{\rm gas} \langle d^{-1} \rangle \approx 1000\,{\rm W/m^2K}.$$

Let us assume that $p_0 \approx 0.01\,{\rm MPa}$, $E^* \approx 2\,{\rm MPa}$, $u_0 \approx 10\,\mu{\rm m}$ and (for rubber) $\kappa_0 = 0.2\,{\rm W/m\,K}$. Thus

$$\alpha_{\rm con} = \frac{p_0 \kappa_0}{E^* u_0} \approx 100\,{\rm W/m^2K}.$$

Here we have used that $\kappa \approx \kappa_0$ (since the heat conductivity κ_1 of copper is much higher than for the rubber). Finally, assuming that the radiative heat transfer is well approximated by the Stefan-Boltzmann law and assuming that $(T_0 - T_1)/T_1 \ll 1$, we get with $T_0 = 373\,{\rm K}$

$$\alpha_{\rm rad} \approx \frac{\pi^2 k_{\rm B}^4}{60 \hbar^3 c^2} 4 T_0^3 \approx 10\,{\rm W/m^2K}.$$

Note that $\alpha_{\rm rad}$ is independent of the squeezing pressure p_0, while $\alpha_{\rm con} \sim p_0$. The pressure dependence of $\alpha_{\rm gas}$ will be discussed below.

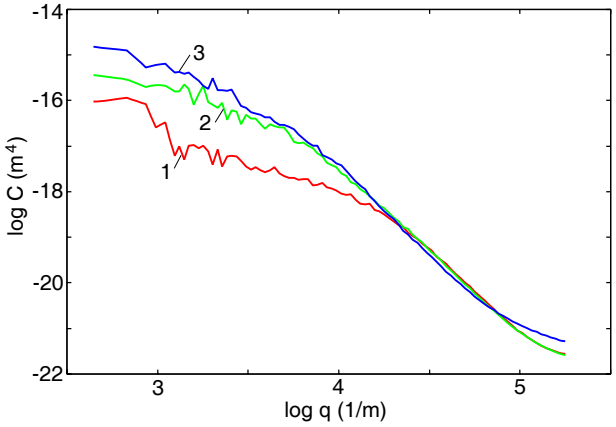

Fig. 14. The surface roughness power spectrum of the three copper surfaces used in the experiment. The surfaces **1**, **2** and **3** have the root-mean-square roughness 42, 88 and 114 μm, respectively.

In the experiment reported on below the silicon rubber film has the thickness $d_0 = 2.5\,{\rm mm}$ so that $d_0^{-1}\kappa_0 \approx 100\,{\rm W/m^2K}$. Thus

$$\frac{1}{d_0^{-1}\kappa_0} + \frac{1}{\alpha} \approx \left(\frac{1}{100} + \frac{1}{1000 + 100 + 10} \right) ({\rm W/m^2K})^{-1}$$

and it is clear from this equation that in the present case the thin rubber film will give the dominant contribution to the heat resistance. This is in accordance with our experimental data presented below.

8 Experimental results and discussion

To test the theory we have performed the experiment described in sect. 7. We have performed experiments on four different (copper) substrate surfaces, namely one highly polished surface (surface **0**) with the root-mean-square (rms) roughness 64 nm, and for three rough surfaces with the rms roughness 42, 88 and 114 μm. In fig. 14 we show the surface roughness power spectrum of the three latter surfaces. Including only the roughness with wavelength above $\sim 30\,\mu$m, the rms slope of all three surfaces are of order unity, and the normalized surface area $A/A_0 \approx 1.5$ in all cases.

In fig. 15 we show for the surfaces **1**, **2** and **3**, the pressure dependence of heat transfer coefficient from the contact area ($\alpha_{\rm con}$) and from the air-gap ($\alpha_{\rm gas}$). In calcultating the results in fig. 15 we have used (26a) (with u_0 from (60)) (top figure) and (46) (with $P(u)$ from (56a)) (bottom figure). Note that both $\alpha_{\rm con}$ and $\alpha_{\rm gas}$ varies (nearly) linearly with p_0. The latter may at first appear remarkable because we know that at the low (nominal) squeezing pressures used in the present calculation (where the area of real contact varies linearly with p_0), the average surface separation $\bar{u} = \langle u \rangle$ depends logarithmically on p_0. However, the heat transfer via heat diffusion in the air gap depends on $\langle (u + \Lambda)^{-1} \rangle$, which depends on p_0 almost linearly as long as $\bar{u} \gg \Lambda$, which is obeyed in our

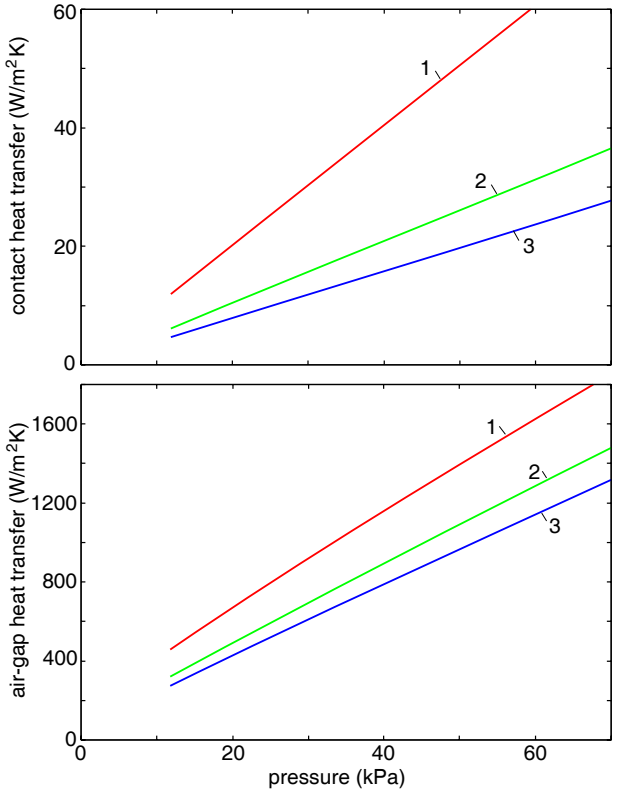

Fig. 15. The variation of the heat transfer coefficient from the contact area ($\alpha_{\rm con}$) and from the air-gap ($\alpha_{\rm gas}$) with the squeezing pressure. The surfaces **1**, **2** and **3** have the power spectra shown in fig. 14.

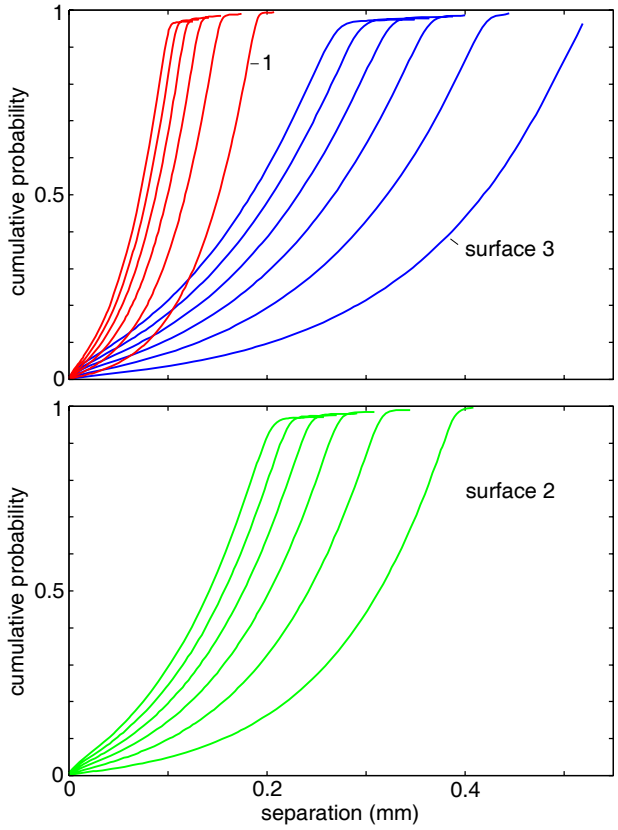

Fig. 16. The variation of the cumulative probability with the height (or gap-separation) u. The surfaces **1** and **3** (top) and **2** (bottom) have the power spectra shown in fig. 14. For each surface the curves are for the nominal squeezing pressures (from right to left): 11.8, 23.7, 35.5, 47.3, 59.2 and 71.0 kPa.

case. This can be understood as follows: $\langle u\rangle$ is determined mainly by the surface regions where the surface separation is close to its largest value. On the other hand $\langle(u+\Lambda)^{-1}\rangle$ is determined mainly by the surface regions where u is very small, *i.e.*, narrow strips (which we will refer to as boundary strips) of surface area close to the area of real contact. Now, for small p_0 the area of real contact increases linearly with p_0 while the distribution of sizes of the contact regions is independent of p_0. It follows that the total area of the boundary strips will also increase linearly with p_0. Thus, since $\langle(u+\Lambda)^{-1}\rangle$ is determined mainly by this surface area, it follows that $\langle(u+\Lambda)^{-1}\rangle$ will be nearly proportional to p_0. We note that, in fig. 9, $\alpha_{\rm gas}$ is nearly pressure independent, but this is due to the fact that the (combined) surface in this case is extremely smooth (root-mean-square roughness 2.5 nm) so that the u-term in $\langle(u+\Lambda)^{-1}\rangle$ can be neglected compared to the gas mean free path Λ, giving a nearly pressure-independent gas heat transfer coefficient. However, in the system studied above $\bar{u}$ is much larger than Λ and the result is nearly independent of Λ.

Note that in the present case (see fig. 15) $\alpha_{\rm gas} \gg \alpha_{\rm con}$, so that the present experiment mainly tests the theory for the heat flow in the air gap.

In fig. 16 we show the variation of the cumulative probability with the height (or gap-separation) u for the surfaces **1** and **3** (top) and **2** (bottom).

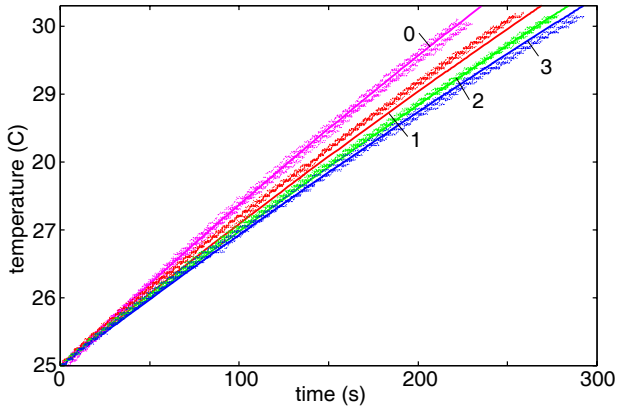

Fig. 17. The measured (dots) and calculated (solid lines) temperature in the lower container as a function of time. Results are for all four surfaces and for the nominal squeezing pressure $p_0 = 0.012$ MPa.

In fig. 17 we show the measured (dots) and calculated (using (70b)) (solid lines) temperature in the lower container as a function of time. Results are for all four surfaces and for the nominal squeezing pressure $p_0 = 0.012$ MPa. The experiments where repeated 16 times and all the experimental data points are shown in the figure. In fig. 18

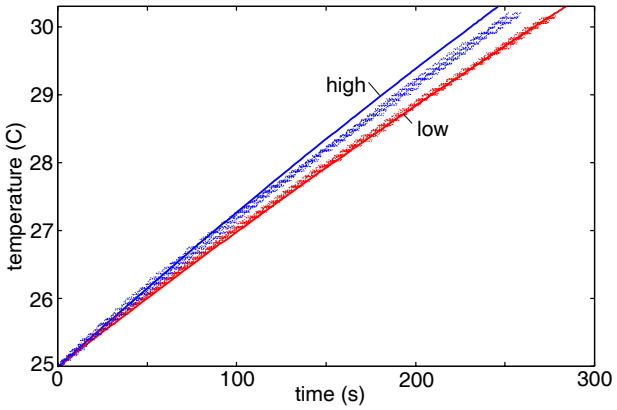

Fig. 18. The measured (dots) and calculated (solid lines) temperature in the lower container as a function of time. Results are for surface **2** for the nominal squeezing pressure $p_0 = 0.012$ (lower curve) and 0.071 MPa (upper curve).

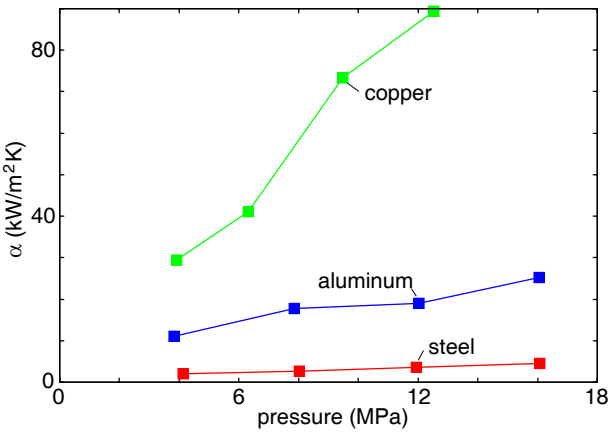

Fig. 19. Variation of the heat transfer coefficient α with the squeezing pressure p_0 for metal-metal contact with steel, copper and aluminum. The surfaces have the effective (or combined) root-mean-square surface roughness values $h_{\rm rms} = 7.2\,\mu$m (steel), $2.2\,\mu$m (copper) and $5.0\,\mu$m (aluminum). The heat conductivity of the metals are $\kappa = 54\,{\rm W/m\,K}$ (steel), $381\,{\rm W/m\,K}$ (copper) and $174\,{\rm W/m\,K}$ (aluminum). Based on experimental data from ref. [42].

we show the measured (dots) and calculated (solid lines) temperature in the lower container as a function of time. Results are for surface **2** for the nominal squeezing pressure $p_0 = 0.012$ (lower curve) and 0.071 MPa (upper curve). Note that there is no fitting parameter in the theory calculations, and the agreement between theory and experiment is relatively good.

It would be interesting to repeat the experiment presented above under vacuum condition. In this case about half of the heat transfer resistance will arise from heat diffusion in the thin rubber film and half arises from the area of real contact, and it would be easy to accurately test the theory for the latter contribution. It would also be interesting to repeat the experiment using elastic materials with thermal conductivities much higher than that of silicon rubber.

The heat resistance of the system studied above is dominated by the thin rubber film. The reason for this is the low heat conductivity of rubber (roughly 100 times lower than for metals). For direct metal-metal contact the contact resistance will be much more important. However, for very rough surfaces it is likely that plastic flow is observed already at such low magnification (corresponding to large length scales) that it will affect the contact resistance. Nevertheless, it is interesting to compare the theory predictions for elastic contact with experimental data for metal-metal contacts.

In fig. 19 we show the measured heat transfer coefficient for metal-metal contacts with steel, copper and aluminum [42]. The surfaces have the effective (or combined) rms surface roughness $h_{\rm rms} = 7.2\,\mu$m (steel), $2.2\,\mu$m (Cu) and $5.0\,\mu$m (Al). Assume that the variation of α with p_0 is mainly due to the area of real contact, *i.e.*, we neglect the heat transfer via the thin air film between the surfaces. For the experiments involving rubber discussed above, the contribution to the heat transfer coefficient α from the area of real contact was smaller by a factor of ~ 20 than the contribution from heat diffusion in the air gap, but because of the much higher thermal conductivity of metals (typically $\sim$ 100–1000 times higher) the contribution to α from the area of real contact (which is proportional to κ) will be much more important. Fitting the data points in fig. 19 with straight lines gives the slope ${\rm d}\alpha/{\rm d}p_0({\rm exp})$ (in units of m/s K)

$$2 \times 10^{-4}\ \text{(steel)}, \qquad 7 \times 10^{-3}\ \text{(Cu)}, \qquad 1.2 \times 10^{-3}\ \text{(Al)}.$$

Using (26a) with $u_0 \approx 0.4 h_{\rm rms}$ (here we have assumed $\gamma = 0.4$) gives ${\rm d}\alpha/{\rm d}p_0({\rm theory}) = \kappa/E^* u_0$

$$1 \times 10^{-4}\ \text{(steel)}, \qquad 4 \times 10^{-3}\ \text{(Cu)}, \qquad 1.3 \times 10^{-3}\ \text{(Al)}$$

The agreement between theory and experiment is very good taking into account that plastic deformation may have some influence on the result, and that an accurate analysis requires the full surface roughness power spectrum $C(q)$ (in order to calculate u_0 accurately, and in order to include plastic deformation if necessary (see sect. 5)), which was not reported on in ref. [42]. We note that experimental results such as those presented in fig. 19 are usually analyzed with a phenomenological model which assumes plastic flow and neglects elastic deformation. In this theory the heat transfer coefficient [43]

$$\alpha \approx \frac{\kappa s p_0}{h_{\rm rms}\sigma_{\rm Y}} \tag{71}$$

is proportional to the rms *surface slope* s, but it is well known that this quantity is dominated by the very shortest wavelength roughness which in fact makes the theory ill-defined. In ref. [42] the data presented in fig. 19 was analyzed using (71) with $s = 0.035$, 0.006 and 0.03 for the steel, Cu and Au surfaces, respectively. However, analysis of polished surfaces with similar rms roughness as used in the experiments usually gives slopes of order unity when all roughness down to the nanometer is included in the analysis [44]. Using $s \approx 1$ in (71) gives heat transfer coefficients roughly ~ 100 times larger than observed in the

experiments. (In our theory (eq. (26a)) $s/\sigma_{\rm Y}$ in (71) is replaced with $1/E^*$, and since typically $E^*/\sigma_{\rm Y} \approx 100$, our theory is consistent with experimental observations.) [45] We conclude that the theory behind (71) is incorrect or incomplete. A theory which includes both elastic and plastic deformation was described in sect. 5.

9 Electric contact resistance

It is easy to show that the problem of the electrical contact resistance is mathematically equivalent to the problem of the thermal contact resistance. Thus, the electric current (per unit nominal contact area) J_0 through an interface between solids with randomly rough surfaces can be related to the electric potential drop $\Delta\phi$ at the interface via $J_0 = \alpha' \Delta\phi$ where, in analogy with (25),

$$\alpha' = \frac{p_0 \kappa'}{E^* u_0}\,, \tag{72}$$

where κ' is the electrical conductivity. However, from a practical point of view the problem of the electrical contact resistance is more complex than for the heat contact resistance because of the great sensitivity of the electric conductivity on the type of material (see Appendix E). Thus, in a metal-metal contact the contact resistance will depend sensitively on whether the thin insulating oxide layers, which cover most metals, are fractured, so that direct metal-metal contact can occur. On the other hand, in most cases there will be a negligible contribution to the electric conductivity from the non-contact regions.

10 Summary and conclusion

We have studied the heat transfer between elastic solids with randomly rough but nominally flat surfaces squeezed in contact with the pressure p_0. Our approach is based on studying the heat flow and contact mechanics in wave vector space rather than real space which has the advantage that we do not need to consider the very complex fractal-like shape of the contact regions in real space. We have included both the heat flow in the area of real contact as well as the heat flow across the non-contact surface region. For the latter contribution we have included the heat transfer both from the fluctuating electromagnetic field (which surrounds all material objects), and the heat flow via the surrounding gas or liquid. We have also studied the contribution to the heat transfer from capillary bridges, which form spontaneously in a humid atmosphere (*e.g.*, as a result of organic and water contamination films which occur on most solid surfaces in the normal atmosphere). We have presented an illustrative application relevant for MEMS applications involving very smooth amorphous silicon dioxide surfaces. In this case we find that all the mentioned heat transfer processes may be roughly of equal importance.

We have briefly discussed the role of plastic deformation and adhesion on the contact heat resistance. We have pointed out that even if plastic deformation and adhesion are important at short length scale (or high magnification) they may have a negligible influence on the heat transfer since the elastic energy stored in the asperity contact regions, which mainly determines both the interfacial separation and the contact heat transfer coefficient, is usually mainly determined by the long-wavelength surface roughness components, at least for fractal-like surfaces with fractal dimension $D_{\rm f} < 2.5$ (which is typically obeyed for natural surfaces and surfaces of engineering interest).

We thank Christian Schulze (ISAC, RWTH Aachen University) for help with the measurement of the surface topography of the copper surfaces. A.I.V. acknowledges financial support from the Russian Foundation for Basic Research (Grant N 08-02-00141-a) and from DFG. This work, as part of the European Science Foundation EUROCORES Program FANAS, was supported from funds by the DFG and the EC Sixth Framework Program, under contract N ERAS-CT-2003-980409.

Appendix A.

In sect. 2.2.1 we have assumed that

$$\frac{1}{J_0^2}\int {\rm d}^2q \frac{1}{q}\langle|\Delta J_z(\mathbf{q})|^2\rangle \approx \frac{1}{p_0^2}\int {\rm d}^2q \frac{1}{q}\langle|\Delta\sigma_z(\mathbf{q})|^2\rangle. \tag{A.1}$$

This equation is a consequence of the fact that for elastic solids with randomly rough surfaces the heat transfer coefficient depends mainly on the geometrical distribution of the contact area. This can be understood as follows. Let $\mathbf{x}_n$ denote the center of the contact spot n and let I_n be the heat current through the same contact spot. We now approximate

$$J_z(\mathbf{x}) \approx \sum_n I_n \delta(\mathbf{x} - \mathbf{x}_n).$$

Thus

$$A_0 J_0 = \sum_n I_n$$

and

$$J_z(\mathbf{q}) = \frac{1}{(2\pi)^2}\sum_n I_n e^{-i\mathbf{q}\cdot\mathbf{x}_n}.$$

Thus the left-hand side (LHS) of (A.1) becomes

$$\begin{aligned}{\rm LHS} \approx & \left(\frac{A_0}{(2\pi)^2}\right)^2 \left(\sum_n I_n\right)^{-2} \\ & \times {\sum_{mn}}' I_n I_m \int {\rm d}^2q\, \frac{1}{q} e^{i\mathbf{q}\cdot(\mathbf{x}_m - \mathbf{x}_n)},\end{aligned} \tag{A.2}$$

where the prime on the summation indicates that the term $m = n$ is excluded from the sum. Next note that

$$\int {\rm d}^2q\, \frac{1}{q} e^{i\mathbf{q}\cdot(\mathbf{x}_m - \mathbf{x}_n)} = \frac{4\pi}{|\mathbf{x}_m - \mathbf{x}_n|}\,. \tag{A.3}$$

Substituting (A.3) in (A.2) gives

$$\mathrm{LHS} \approx \frac{A_0^2}{4\pi^3}\left(\sum_n I_n\right)^{-2} {\sum_{mn}}' \frac{I_m I_n}{|\mathbf{x}_m - \mathbf{x}_n|}\,. \tag{A.4}$$

If one assumes that there is no correlation between the magnitude of I_n (determined by the size of the contact) and its position, we can replace the individual current I_n in the double summation in (A.2) by their mean and get

$$\mathrm{LHS} \approx \frac{1}{4n^2\pi^3} {\sum_{mn}}' \frac{1}{|\mathbf{x}_m - \mathbf{x}_n|}\,, \tag{A.5}$$

where $n = N/A_0$ is the concentration of contact spots and N the total number of contact spots.

In the same way as above, one can simplify the expression involving the normal stress (right-hand side (RHS) of (A.1)). We write

$$\sigma(\mathbf{x}) = \sum_n f_n \delta(\mathbf{x} - \mathbf{x}_n),$$

where f_n is the normal force acting in the contact n. Using this equation, the RHS of (A.1) becomes

$$\mathrm{RHS} \approx \frac{A_0^2}{4\pi^3}\left(\sum_n f_n\right)^{-2} {\sum_{mn}}' \frac{f_m f_n}{|\mathbf{x}_m - \mathbf{x}_n|}\,. \tag{A.6}$$

If one assumes that there is no correlation between the magnitude of f_n and its position, we can replace the individual current f_n in the double summation in (A.6) by their mean and get

$$\mathrm{RHS} \approx \frac{1}{4n^2\pi^3} {\sum_{mn}}' \frac{1}{|\mathbf{x}_m - \mathbf{x}_n|}\,. \tag{A.7}$$

Thus, LHS ≈ RHS and we have proved the (approximate) equality (A.1).

Substituting (A.5) in (20) gives

$$\frac{1}{\alpha} \approx \frac{1}{\pi\kappa n}\frac{1}{N} {\sum_{mn}}' \frac{1}{|\mathbf{x}_m - \mathbf{x}_n|}\,, \tag{A.8}$$

which agrees with the result obtained by Greenwood [23]. We refer to the article of Greenwood for an interesting discussion about the contact resistance based on the (approximate) expression (A.8) for the contact resistance.

Appendix B.

The normal (interfacial) stress $\sigma_z(\mathbf{x})$ and the difference in the surface displacement $u_{0z}(\mathbf{x}) - u_{1z}(\mathbf{x})$ at the interface can be considered to depend on the average interfacial separation $\bar{u}$. The derivatives of these quantities with respect to $\bar{u}$ are denoted by σ_z' and ϕ. In Appendix C we show that

$$\phi(\mathbf{q}) = \delta(\mathbf{q}) - \frac{2}{E^* q}\Delta\sigma_z'(\mathbf{q}). \tag{B.1}$$

Note that (15) and (B.1) are very similar. Thus, if we multiply both sides of (B.1) by M and define $M\phi = \psi$, then (B.1) takes the form

$$\psi(\mathbf{q}) = M\delta(\mathbf{q}) - \frac{\mu}{\kappa q}\Delta\sigma_z'(\mathbf{q}), \tag{B.2}$$

where

$$\mu = \frac{2M\kappa}{E^*} \tag{B.3}$$

Equation (B.2) is identical to (15) if we write

$$J_z(\mathbf{q}) = \mu\sigma_z'(\mathbf{q}), \tag{B.4}$$

or, equivalently,

$$J_z(\mathbf{x})/J_0 = \sigma_z'(\mathbf{x})/p_0',$$

where p_0' is the normal stiffness. We note that (B.4) implies that the current density $J_z(\mathbf{x})$ will be non-vanishing exactly where the normal stress $\sigma_z(\mathbf{x})$ is non-vanishing, which must be obeyed in the present case, where all the heat current flows through the area of real contact. However, in order for $J_z(\mathbf{x})$ to be proportional to $\sigma_z'(\mathbf{x})$, it is not enough that these functions obey similar (in the sense discussed above) differential equations, but both problems must also involve similar boundary conditions. Now in the area of non-contact both J_z and σ_z and hence σ_z' must vanish. In the area of real contact the temperature field T is continuous so that $\psi = T(\mathbf{x}, -0) - T(\mathbf{x}, +0) = 0$, while the displacement field satisfies $\Phi = u_{0z} - u_{1z} = h(\mathbf{x})$, so that (since $h(\mathbf{x})$ is independent of $\bar{u}$) $\phi = 0$ in the area of real contact. Thus, both problems involve the same boundary conditions and J_z and σ_z' must therefore be proportional to each other.

Note that (B.4) gives $J_0 = \mu p_0'$. Substituting (B.3) in this equation and using the definition (16) gives an equation of the form (3) with

$$\alpha = -\frac{\kappa}{E^*}\frac{\mathrm{d}p_0}{\mathrm{d}\bar{u}}\,.$$

This *exact* relation between the heat transfer coefficient and the normal stiffness per unit area has already been derived by Barber [24] using a somehow different approach.

Appendix C.

In refs. [10,11] it was shown that the normal displacement u_{0z} is related to the normal stress σ_z via

$$u_{0z}(\mathbf{q}) = -\frac{2}{E_0^* q}\sigma_z(\mathbf{q}), \tag{C.1}$$

where $E_0^* = E_0/(1-\nu_0^2)$. In a similar way

$$u_{1z}(\mathbf{q}) = \frac{2}{E_1^* q}\sigma_z(\mathbf{q}). \tag{C.2}$$

Let $\Phi = u_{0z} - u_{1z}$ be the difference between the (interfacial) surface displacement fields. Using (C.1) and (C.2) gives

$$\Phi(\mathbf{q}) = -\frac{2}{E^* q}\sigma_z(\mathbf{q}) \tag{C.3}$$

where

$$\frac{1}{E^*} = \frac{1}{E_0^*} + \frac{1}{E_1^*}\,.$$

Note that the average of $\Phi(\mathbf{x})$ is the average separation between the surfaces which we denote by $\bar{u}$. Thus if

$$\sigma_z(\mathbf{x}) = p_0 + \Delta\sigma_z(\mathbf{x}),$$

we get

$$\Phi(\mathbf{q}) = \bar{u}\delta(\mathbf{q}) - \frac{2}{E^* q}\Delta\sigma_z(\mathbf{q}). \qquad \text{(C.4)}$$

As the squeezing pressure p_0 increases, the average separation $\bar{u}$ will decrease and we can consider p_0 as a function of $\bar{u}$. The quantity $p_0'(\bar{u})$ is referred to as the normal stiffness per unit nominal contact area. Taking the derivative of (C.4) with respect to $\bar{u}$ gives

$$\phi(\mathbf{q}) = \delta(\mathbf{q}) - \frac{2}{E^* q}\Delta\sigma_z'(\mathbf{q}), \qquad \text{(C.5)}$$

where σ_z' is the derivative of σ_z with respect to $\bar{u}$ and where $\phi = \Phi'$ is the derivative of Φ with respect to $\bar{u}$.

Appendix D.

Here we briefly summarize some results related to forced convective heat transfer [46]. When a fluid (*e.g.*, air) flows around a solid object the tangential (and the normal) component of the fluid velocity usually vanish on the surface of the solid. This results in the formation of a thin boundary layer (thickness δ) at the surface of the solid where the fluid velocity rapidly increases from zero to some value which is of order the main stream velocity outside of the solid. If the temperature T_1 at the solid surface is different from the fluid temperature $T_{\rm fluid}$, the fluid temperature in the boundary layer will also change rapidly from T_1 to $T_{\rm fluid}$. Depending on the fluid flow velocity, the fluid viscosity and the dimension of the solid object, the flow will be laminar or turbulent, and the heat transfer process is fundamentally different in these two limiting cases. In a typical case (for air) the thickness $\delta \approx 1\,{\rm mm}$ and the heat transfer coefficient $\alpha \approx \kappa/\delta \approx 10\,{\rm W/m^2K}$.

Let us consider heat transfer from a rotating disk as a model for the heat transfer from a tire [47]. In this case it has been shown [48] that fully turbulent flow occurs if the Reynolds number ${\rm Re} > 2.5 \times 10^5$, where

$${\rm Re} = \frac{\omega R^2}{\nu} = \frac{v_{\rm R} R}{\nu}\,,$$

where R is the radius of the disk (or rather the distance from the center of the disk to some surface patch on the disk), ω the angular velocity and ν the kinematic viscosity of air. In typical tire applications ${\rm Re} > 2.5 \times 10^5$ so turbulent flow will prevail in most tire applications. In this case the heat transfer coefficient is given approximately by [48]

$$\alpha_{\rm air} \approx 0.019 \frac{\kappa_{\rm air}}{R} \left(\frac{v_{\rm R} R}{\nu}\right)^{0.8}\,.$$

As an example, at $T = 300\,{\rm K}$ for air $\nu = 15.7 \times 10^{-6}\,{\rm m^2/s}$ and $\kappa_{\rm air} = 0.025\,{\rm W/m\,K}$ and assuming $R = 0.3\,{\rm m}$ and $v_{\rm R} = 30\,{\rm m/s}$, we get $\alpha_{\rm air} \approx 63\,{\rm W/m^2K}$.

Appendix E.

Heat conduction results from the collisions between atoms as in fluids, or by free electron diffusion as predominant in metals, or phonon diffusion as predominant in insulators. In liquids and gases, the molecules are usually further apart than in solids, giving a lower chance of molecules colliding and passing on thermal energy. Metals are usually the best conductors of thermal energy. This is due to the free-moving electrons which are able to transfer thermal energy rapidly through the metal. However, the difference in the thermal conductivity of metals and non-metals are usually not more than a factor ~ 100. Typical values for the heat conductivity are $\kappa \approx 100\,{\rm W/m\,K}$ for metals, $\approx 1\,{\rm W/m\,K}$ for insulators (*e.g.*, metal oxides or polymers), $\approx 0.1\,{\rm W/m\,K}$ for fluids (but for water $\kappa \approx 0.6\,{\rm W/m\,K}$) and $\approx 0.02\,{\rm W/m\,K}$ for gases at normal atmospheric pressure and room temperature.

In contrast to thermal heat transfer, electric conduction always involves the motion of charged particles (electrons or ions). For this reason the electric contact resistance is much more sensitive to oxide or contamination layers at the contacting interface than for the heat transfer. For the electric conduction the variation of conductivity between good conductors (most metals), with typical electric conductivity $\kappa' \approx 10^7\ (\Omega\,{\rm m})^{-1}$, and bad conductors such as silicon dioxide glass or (natural) rubber, where $\kappa' \approx 10^{-14}\ (\Omega\,{\rm m})^{-1}$, is huge. This makes the electrical contact resistance of metals sensitive to (nanometer) thin oxide or contamination layers. However, as pointed out in the Introduction, if there is a large number of small breaks in the film, the resistance may be almost as low as with no film.

References

1. B.N.J. Persson, J. Phys.: Condens. Matter **18**, 7789 (2006).
2. For a review of thermal joint resistance models for rough surfaces, see, *e.g.*, M. Bahrami, J.R. Culham, M.M. Yovanovich, G.E. Schneider, Appl. Mech. Rev. **59**, 1 (2006).
3. J.A. Greenwood, J.B.P. Williamson, Proc. R. Soc. London, Ser. A **295**, 300 (1966).
4. A.W. Bush, R.D. Gibson, T.R. Thomas, Wear **35**, 87 (1975).
5. C. Campana, M.H. Müser, M.O. Robbins, J. Phys.: Condens. Matter **20**, 354013 (2008).
6. G. Carbone, F. Bottiglione, J. Mech. Phys. Solids **56**, 2555 (2008).
7. See also Appendix A in B.N.J. Persson *et al.*, J. Phys.: Condens. Matter **20**, 395006 (2008).
8. B.N.J. Persson, J. Phys.: Condens. Matter **20**, 312001 (2008).
9. B.N.J. Persson, F. Bucher, B. Chiaia, Phys. Rev. B **65**, 184106 (2002).
10. B.N.J. Persson, J. Chem. Phys. **115**, 3840 (2001).
11. B.N.J. Persson, Eur. Phys. J. E **8**, 385 (2002).
12. B.N.J. Persson, Phys. Rev. Lett. **99**, 125502 (2007).
13. C. Yang, B.N.J. Persson, J. Phys.: Condens. Matter **20**, 215214 (2008).

14. B.N.J. Persson, Surf. Sci. Rep. **61**, 201 (2006).
15. B.N.J. Persson, C. Yang, J. Phys.: Condens. Matter **20**, 315011 (2008).
16. M. Borri-Brunetto, B. Chiaia, M. Ciavarella, Comput. Methods Appl. Mech. Eng. **190**, 6053 (2001).
17. L. Pei, S. Hyun, J.F. Molinari, M.O. Robbins, J. Mech. Phys. Solids **53**, 2385 (2005).
18. See, *e.g.*, B.N.J. Persson, O. Albohr, U. Tartaglino, A.I. Volokitin, E. Tosatti, J. Phys.: Condens. Matter **17**, R1 (2005).
19. B.N.J. Persson, *Sliding Friction: Physical Principles and Applications*, 2nd edition (Springer, Heidelberg, 2000).
20. C. Yang, U. Tartaglino, B.N.J. Persson, Eur. Phys. J. E **19**, 47 (2006).
21. S. Hyun, L. Pei, J.F. Molinarie, M.O. Robbins, Phys. Rev. E **70**, 026117 (2004).
22. Y.F. Mo, K.T. Turner, I. Szlufarska, Nature **457**, 1116 (2009).
23. J.A. Greenwood, Brit. J. Appl. Phys. **17**, 1621 (1966)
24. J.R. Barber, Proc. R. Soc. London, Ser. A **459**, 53 (2003).
25. J.F. Archard, Wear **2**, 438 (1959).
26. D. Pires, B. Gotsmann, F. Porro, D. Wiesmann, U. Duerig, A. Knoll, Langmuir **25**, 5141 (2009).
27. A.I. Volokitin, B.N.J. Persson, Rev. Mod. Phys. **79**, 1291 (2007).
28. K. Joulain, J.P. Mulet, F. Marquier, R. Carminati, J.J. Greffet, Surf. Sci. Rep. **57**, 59 (2005).
29. D. Segal, A. Nitzan, Chem. Phys. **268**, 315 (2001).
30. D. Segal, A. Nitzan, Chem. Phys. **281**, 235 (2002).
31. Y. Selzer, M.A. Cabassi, T.S. Mayer, D.L. Allara, Nanotechnology **15**, S483 (2004).
32. V. Popov, *Kontaktmechanik und Reibung* (Springer, Heidelberg, 2009).
33. M. Bahrami, J.R. Culham, M.M. Yovanovich, *Proceedings of the International Mechanical Engineering Congress and Exhibition (IMECE)*, ASME paper 44097 (Washington, 2003).
34. D.Z.A. Chen, R. Hamam, M. Soljacic, J.D. Joannopoulos, G. Chen, Appl. Phys. Lett. **90**, 181921 (2007).
35. M. Bahrami, M.M. Yovanovich, J.R. Culham, J. Thermophys. Heat Transfer **18**, 326 (2004).
36. B.N.J. Persson, J. Phys.: Condens. Matter **20**, 315007 (2008).
37. K.L. Johnson, *Contact Mechanics* (Cambridge University Press, Cambridge, 1985).
38. L. Shi, A. Majumdar, J. Heat Transfer **124**, 329 (2002).
39. C. Yang, B.N.J. Persson, J. Israelachvili, K. Rosenberg, Eur. Phys. Lett. **84**, 46004 (2008).
40. In ref. [14] we used $A_{\rm pl}/A_{\rm pl}^0$ instead of $(A_{\rm pl}/A_{\rm pl}^0)^6$ in the expression for $\bar{C}$, but we have found that the latter (more rapid) cut-off, gives better results: The contact area as a function of magnification, for elastic contact with the latter $\bar{C}$, gives virtually the same result as the calculated (total) contact area using the elastoplastic contact mechanics theory and the original surface roughness power spectrum.
41. B.S. Oh, Y.N. Kim, N.J. Kim, H.Y. Moon, H.W. Park, Tire Sci. Technol. **23**, 11 (1995).
42. H. Yüncü, Heat Mass Transfer **43**, 1 (2006).
43. M.M. Yavanovich, AIAA-86-1164, presented at 16th Thermo Physics Conference (1981), Palo Alto, CA, USA.
44. As an example, using AFM we have measured the height profile of a polished steel surface over a $10\,\mu{\rm m} \times 10\,\mu{\rm m}$ surface area with the resolution $a = 20\,{\rm nm}$. From the numerical data we calculated the root-mean-square (rms) roughness $h_{\rm rms} \approx 0.1\,\mu{\rm m}$ and the rms slope $s \approx 0.6$. Increasing the lateral resolution would increase the slope further since the slope is mainly determined by the short-wavelength roughness.
45. It may be argued that, due to plastic deformation, the slope in (71) should be calculated including only the roughness with wavelength above some cut-off length. However, no discussion of this point was presented in ref. [43].
46. L.D. Landau, E.M. Lifshitz, *Fluid Mechanics* (Pergamon Press, Oxford, 1959).
47. J. Mc Allen, A.M. Cuitino, V. Sernas, Finite Elements Anal. Design **23**, 265 (1996).
48. C.O. Popiel, L. Boguslawski, Int. J. Heat Mass Transfer **18**, 170 (1975).